AD-A195 321 COMPUTER SIMULATION STUDIES OF MULTIPLE BROADBAND TARGET LOCALIZATION VIA..(U) NAVAL POSTGRADUATE SCHOOL MONTEREY CA C D BEHRLE MAR 88 1/1

UNCLASSIFIED F/G 17/1 NL

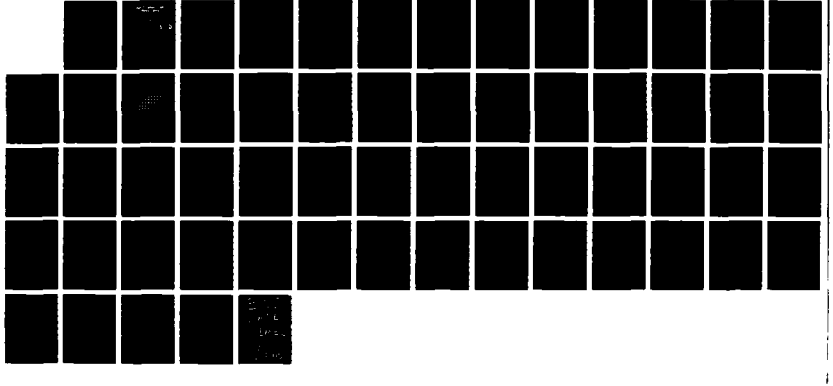

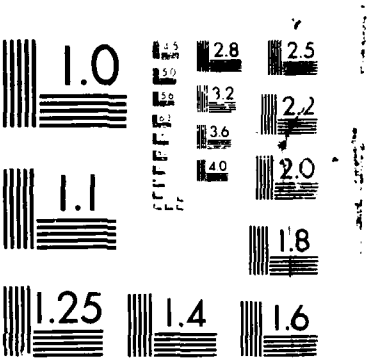


MICROCOPY RESOLUTION TEST CHA
NATIONAL BUREAU OF STANDARDS 1963

DTIC FILE COPY (2)

# NAVAL POSTGRADUATE SCHOOL
## Monterey, California

AD-A195 321


DTIC
ELECTE
JUN 14 1988
S D
H

# THESIS

COMPUTER SIMULATION STUDIES OF MULTIPLE BROADBAND TARGET LOCALIZATION VIA FREQUENCY DOMAIN ADAPTIVE BEAMFORMING FOR PLANAR ARRAYS

by

Charles D. Behrle

March 1988

Thesis Advisor L. J. Ziomek

Approved for public release; distribution is unlimited

# REPORT DOCUMENTATION PAGE

| | |
|---|---|
| 1a. REPORT SECURITY CLASSIFICATION<br>UNCLASSIFIED | 1b. RESTRICTIVE MARKINGS |
| 2a. SECURITY CLASSIFICATION AUTHORITY | 3. DISTRIBUTION/AVAILABILITY OF REPORT<br>Approved for public release; distribution is unlimited |
| 2b. DECLASSIFICATION/DOWNGRADING SCHEDULE | |
| 4. PERFORMING ORGANIZATION REPORT NUMBER(S) | 5. MONITORING ORGANIZATION REPORT NUMBER(S) |
| 6a. NAME OF PERFORMING ORGANIZATION<br>Naval Postgraduate School<br>6b. OFFICE SYMBOL (*If applicable*)<br>62 | 7a. NAME OF MONITORING ORGANIZATION<br>Naval Postgraduate School |
| 6c. ADDRESS (*City, State, and ZIP Code*)<br>Monterey, California 93943-5000 | 7b. ADDRESS (*City, State, and ZIP Code*)<br>Monterey, California 93943-5000 |
| 8a. NAME OF FUNDING/SPONSORING ORGANIZATION<br>8b. OFFICE SYMBOL (*If applicable*) | 9. PROCUREMENT INSTRUMENT IDENTIFICATION NUMBER |
| 8c. ADDRESS (*City, State, and ZIP Code*) | 10. SOURCE OF FUNDING NUMBERS<br>PROGRAM ELEMENT NO / PROJECT NO / TASK NO / WORK UNIT ACCESSION NO |

11. TITLE (*Include Security Classification*)
Computer Simulation Studies of Multiple Broadband Target Localization Via Frequency Domain Adaptive Beamforming for Planar Arrays

12. PERSONAL AUTHOR(S)
Charles D. Behrle

| 13a. TYPE OF REPORT | 13b. TIME COVERED | 14. DATE OF REPORT (*Year, Month, Day*) | 15. PAGE COUNT |
|---|---|---|---|
| Thesis, M.S. | FROM _____ TO _____ | March, 1988 | 58 |

16. SUPPLEMENTARY NOTATION
The views expressed in this thesis are those of the author and do not reflect the official policy or position of the Department of Defense or the U.S. Government.

| 17. COSATI CODES | | | 18. SUBJECT TERMS (*Continue on reverse if necessary and identify by block number*) |
|---|---|---|---|
| FIELD | GROUP | SUB-GROUP | frequency domain adaptive beamforming; signal processing planar array; least mean square error |
| | | | |
| | | | |

19. ABSTRACT (*Continue on reverse if necessary and identify by block number*)

Computer simulation studies of a frequency domain adaptive beamforming algorithm are presented. These simulation studies were conducted to determine the multiple broadband target localization capability and the full angular coverage capability of the algorithm. The algorithm was evaluated at several signal-to-noise ratios with varying sampling rates. The number of iterations that the adaptive algorithm took to reach a minimum estimation error was determined. Results of the simulation studies indicate that the algorithm can localize multiple broadband targets and has full angular coverage capability.

| 20. DISTRIBUTION/AVAILABILITY OF ABSTRACT | 21. ABSTRACT SECURITY CLASSIFICATION |
|---|---|
| ☒ UNCLASSIFIED/UNLIMITED ☐ SAME AS RPT ☐ DTIC USERS | UNCLASSIFIED |
| 22a. NAME OF RESPONSIBLE INDIVIDUAL<br>Professor L. J. Ziomek | 22b. TELEPHONE (*Include Area Code*)<br>408-646-3206 / 22c. OFFICE SYMBOL<br>62Zm |


☆ U.S. Government Printing Office 1986—606-243

Approved for public release; distribution is unlimited

Computer Simulation Studies of Multiple Broadband Target Localization Via Frequency Domain Adaptive Beamforming for Planar Arrays

by

Charles D. Behrle
Lieutenant, United States Navy
B.S., United States Naval Academy, 1980

Submitted in partial fulfillment of the requirements for the degree of

MASTER OF SCIENCE IN ELECTRICAL ENGINEERING

from the

NAVAL POSTGRADUATE SCHOOL
March 1988

Author: Charles D. Behrle
Charles D. Behrle

Approved by: L. J. Ziomek
L. J. Ziomek, Thesis Advisor

M. Tummala
M. Tummala, Second Reader

J. P. Powers, Chairman, Department of Electrical and Computer Engineering

Gordon E. Schacher
Gordon E. Schacher,
Dean of Science and Engineering

## ABSTRACT

Computer simulation studies of a frequency domain adaptive beamforming algorithm are presented. These simulation studies were conducted to determine the multiple broadband target localization capability and the full angular coverage capability of the algorithm. The algorithm was evaluated at several signal-to-noise ratios with varying sampling rates. The number of iterations that the adaptive algorithm took to reach a minimum estimation error was determined. Results of the simulation studies indicate that the algorithm can localize multiple broadband targets and has full angular coverage capability.




| Accession For | |
|---|---|
| NTIS GRA&I | ☑ |
| DTIC TAB | ☐ |
| Unannounced | ☐ |
| Justification | |
| By | |
| Distribution/ | |
| Availability Codes | |
| Dist | Avail and/or Special |
| A-1 | |

## TABLE OF CONTENTS

## LIST OF FIGURES

## LIST OF TABLES

## ACKNOWLEDGEMENTS

The author would like to thank Professor L.J. Ziomek for his assistance and patience during the course of this research. I would also like to thank my wife, Gail, for her encouragement, support, and understanding during the many hours that this work required. None of this would have been possible without her.

# I. INTRODUCTION

This thesis is but a part of an ongoing research project to develop new sonar signal processing algorithms capable of quickly and accurately solving target localization problems. Present technology and doctrine dictate that several lines of bearing to a target be obtained before a sonar fire control solution can be computed. Obtaining these lines of bearing is a time consuming and often dangerous task due to the increased probability of counterdetection and, as a result, evasive maneuvering and defensive action on the part of the target. A sonar system capable of providing timely, accurate target localization while minimizing own ship maneuvering would result in longer firing ranges and, therefore, a reduction of the threat to one's own ship.

Several recent papers [Refs. 1–3] have discussed the application of a complex least-mean-square (LMS) adaptive algorithm [Ref. 4] to bearing estimation problems using a linear array of sensors. When a linear array is used, only a bearing angle $\psi_o$ to the source can be estimated, an estimate of the depression angle $\theta_o$ cannot (Figure 1.1). While an estimate of the bearing angle is useful in the localization problem, a better tool would be an algorithm which provides estimates of both the bearing angle and the depression angle. A frequency domain adaptive beamforming algorithm for planar arrays that solves multiple, broadband target localization problems and provides estimates of both the bearing angles and the depression angles from the center of the planar array to the targets has been developed and initially tested by Ziomek and Chan [Ref. 5].

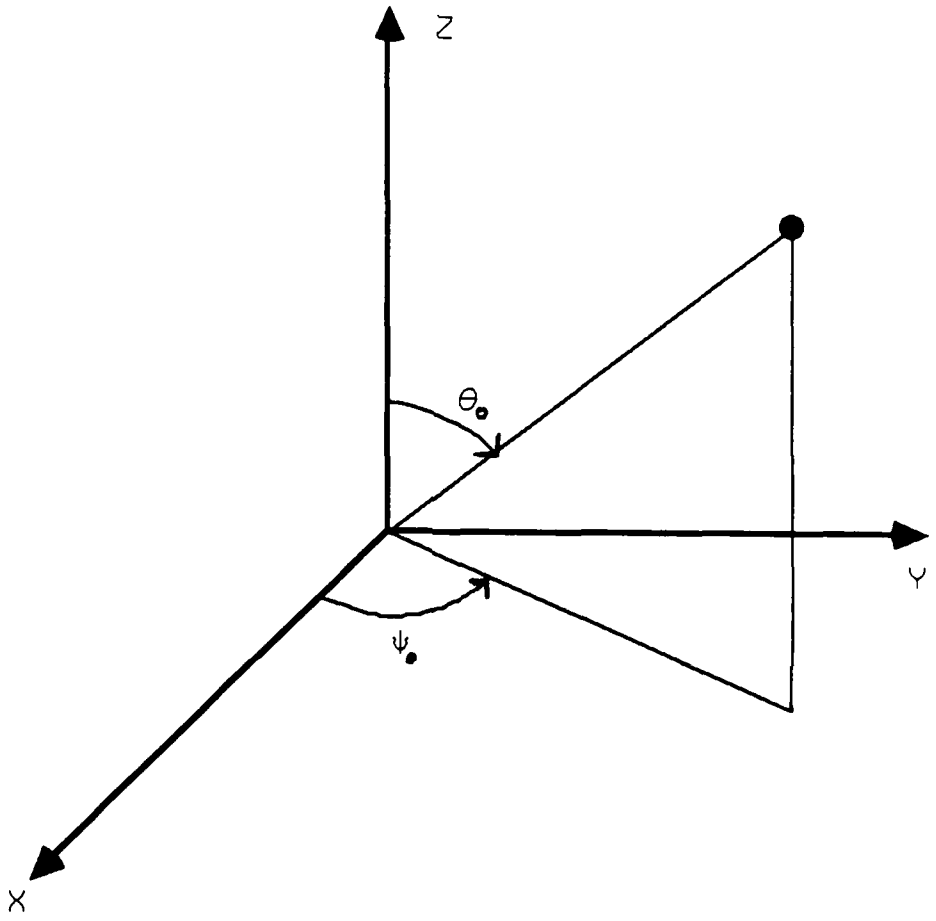


**Figure 1.1. Target Location Geometry.**

The research performed in this thesis was to continue the work of Ziomek and Chan [Refs. 5, 6] and fully evaluate the capabilities of the complex, least-mean-square, frequency domain, adaptive beamforming algorithm they developed via computer simulation studies. The computer simulation studies were designed to test the algorithm's multiple broadband target localization capability, its full angular coverage capability, and its angular resolution as a function of the input signal-to-noise ratio (SNR) at a single element in the array, sampling rate, harmonic number, and the number of iterations of the algorithm.

Each target was modeled as a broadband sound source. As a result, the frequency spectrum of the output signal from each element of the planar array contains several frequency components. An estimate of the bearing and depression angle for each frequency component is provided as a result of processing the output frequency spectrum from each element in the array through the frequency domain adaptive beamforming algorithm. Therefore, if each target exhibits at least one unique frequency component (or spectral line), then all targets can be located.

Full angular coverage is the ability to localize a target regardless of its relative position to the array. The broadside case is the easiest since it is at this position that the far-field beam pattern beamwidth is its narrowest. The endfire case is the most difficult since the far-field beam pattern beamwidth is the broadest at this point. The full angular coverage and multiple broadband target capabilities were tested simultaneously.

Baseline results were the first assembled. Baseline results are defined as bearing and depression angle estimation errors (measured in degrees) as a function of sampling rate, harmonic number, and the number of iterations of the algorithm for the "no noise" case. Identical cases were run using additive, zero mean, white,

guassian noise to corrupt the output signals from each element of the planar array. Average bearing and depression angle estimation errors were then plotted as a function of the input SNR at a single element of the planar array, the sampling rate, and the harmonic number.

Chapter II describes the theory used in the development of the frequency domain adaptive beamforming algorithm. The construction of the direction cosine estimates, the angle estimates, and phase "unwrapping", integral parts of the algorithm, will be presented in detail.

Chapter III contains computer simulation results and an explanation of these results. The results which are presented consist of graphical representations of the average estimation errors of the bearing and depression angles at two distinct signal-to-noise ratio levels for four cases. These cases include targets evaluated at broadside, endfire, random placement, and targets which share a spectral line. Conclusions concerning the effect of harmonic number, sampling rate, number of iterations of the algorithm, and SNR are made. The Appendix contains tabular numerical data for all results.

Chapter IV will present final conclusions and recommendations for further research.

Results of this thesis research work have been incorporated into a research paper by Ziomek and Behrle which was presented at the Twenty-First Annual Asilomar Conference on Signals, Systems, and Computers [Ref. 7].

# II. THEORY

This chapter is designed to present a brief, yet comprehensive, development of the frequency domain adaptive beamforming algorithm which is evaluated in this thesis. The goal of the algorithm is to process the output electrical signals from a planar array of sensors and provide estimates of direction (both bearing and depression angles) and frequency content of the acoustic fields incident upon the array. The development of the algorithm presented here is similar to the analysis section of a paper by Ziomek and Behrle [Ref. 7], but this chapter provides a more detailed explanation for several parts of the algorithm. A more in-depth analysis of the algorithm is provided by Ziomek and Chan [Ref. 5] and Chan [Ref. 6].

The frequency domain adaptive beamforming algorithm is based on using the complex frequency domain data $R(q,m,n)$ from all $M \times N$ elements of a planar array. The objective of the adaptive filter used in the algorithm is for the filter to converge to a set of phase weights such that the array output signal will match a reference signal. From this set of phase weights, estimates of the bearing and depression angles as a function of the harmonic number $q$ can be made.

Consider a $M \times N$ planar array of point source elements lying in the $XY$ plane (Figure 2.1). These elements are equally spaced where $d_x$ and $d_y$ are the interelement spacings in the $X$ and $Y$ directions, respectively, and $M$ and $N$ are the total number (odd) of elements in the $X$ and $Y$ directions, respectively. The random baseband output electrical signal, $r(\ell,m,n)$, is composed of a deterministic signal, $y(\ell,m,n)$, and a random receiver noise component, $n(\ell,m,n)$. The output signal at time instant $\ell$ and element $(m,n)$ in the array is given by

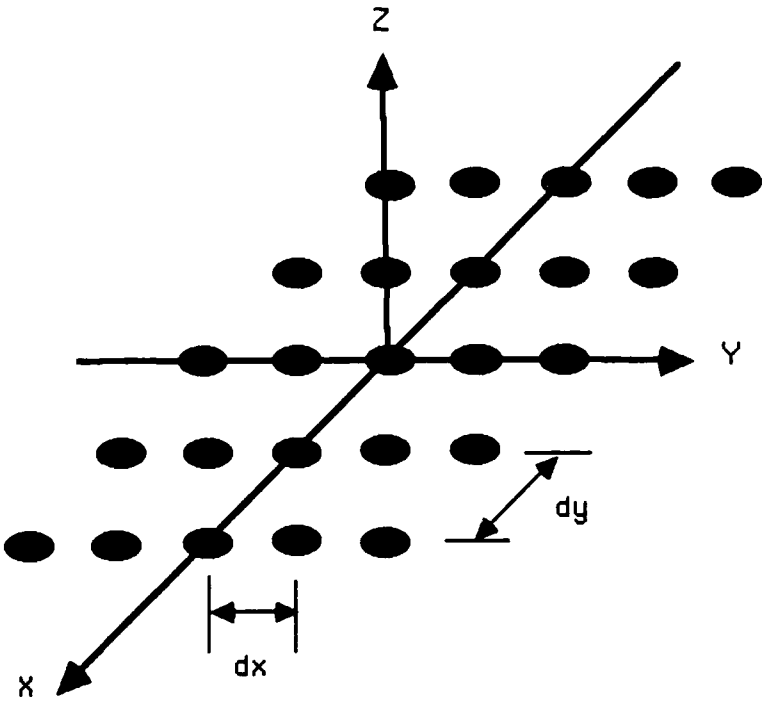


**Figure 2.1. Planar Array Geometry.**

$$r(\ell,m,n) = y(\ell,m,n) + n(\ell,m,n), L = -L', \ldots, 0, \ldots L'$$
$$m = -M', \ldots, 0, \ldots, M' \qquad (2.1)$$
$$n = -N', \ldots, 0, \ldots, N'$$

where

$$L' = (L-1)/2, \qquad (2.2)$$

$$M' = (M-1)/2, \qquad (2.3)$$

$$N' = (N-1)/2, \qquad (2.4)$$

and

$$L \geq 2K+1 \qquad (2.5)$$

is the total number of time samples that must be taken per element to avoid aliasing when the deterministic signal $y(\ell,m,n)$ is composed of $K$ harmonics [Ref. 8: p. 164]. The minimum value for $L$ (i.e., $L = 2K+1$) is obtained by sampling at the Nyquist Rate. If $T_o$ seconds is the length of the data record (or fundamental period) recorded at each element of the array, then the fundamental frequency (or the FFT bin spacing) is given by

$$f_0 = 1/T_0 \text{ Hz.} \qquad (2.6)$$

Therefore, the highest frequency which can be contained within the deterministic part of the received signal is

$$f_{max} = Kf_0 \text{ Hz} \qquad (2.7)$$

and the minimum sampling frequency of the received output electrical signal $r(\ell,m,n)$ is

$$f_S = L/T_0 \text{ Samples/sec} \qquad (2.8)$$

where $L$ must satisfy equation 2.5 [Ref. 8: p. 164].

To obtain the complex frequency domain samples of the received signal, the discrete Fourier transform (DFT) with respect to the time index $\ell$ of equation (2.1) is taken. This action yields

$$R(q,m,n) = Y(q,m,n) + N(q,m,n), q = -L', \ldots, 0, \ldots, L'$$
$$m = -M', \ldots, 0, \ldots, M' \qquad (2.9)$$
$$n = -N', \ldots, 0, \ldots, N'$$

where the index $q$ represents the harmonic number.

Consider a single general plane-wave field, $g\left(t \mp \frac{\underline{r}\cdot\hat{n}_0}{c}\right)$, propagating in the $\pm\hat{n}_0$ direction, incident upon the planar array as shown in Figure 2.2. If $\underline{\hat{n}}_0$ is a unit vector, $g(t)$ an arbitrary baseband function, and $c$ the speed of sound in the medium measured in meters per second, then the deterministic part of the output electrical signal at time instant $\ell$ and element $(m,n)$ in the array is given by [Ref. 8: p. 160]

$$y(\ell,m,n) = g\left(\ell T_S \mp \frac{u_0 m d_X + v_0 n d_Y}{c}\right) \qquad (2.10)$$

where $T_S$ is the sampling period in seconds, and $u_0$ and $v_0$ are dimensionless direction cosines with respect to the $X$ and $Y$ axes, respectively.

Upon taking the DFT of equation 2.10, we obtain the corresponding frequency spectrum given by [Ref. 8: pp. 162-166]

$$Y(q,m,n) = Lc_q \exp(\mp j2\pi q f_0 u_0 m d_X/c)\exp(\mp j2\pi q f_0 v_0 n d_Y/c) \qquad (2.11)$$

where $c_q,\ q = -L', \ldots, 0, \ldots, L'$ are the complex Fourier series coefficients that can be used to represent the baseband function $g(t)$ by a finite Fourier series with $K$ harmonics during the time interval $|t| \geq T_0/2$. The coefficients are given by

$$c_q = Y(q,0,0)/L,\ q = -L', \ldots, 0, \ldots, L'. \qquad (2.12)$$

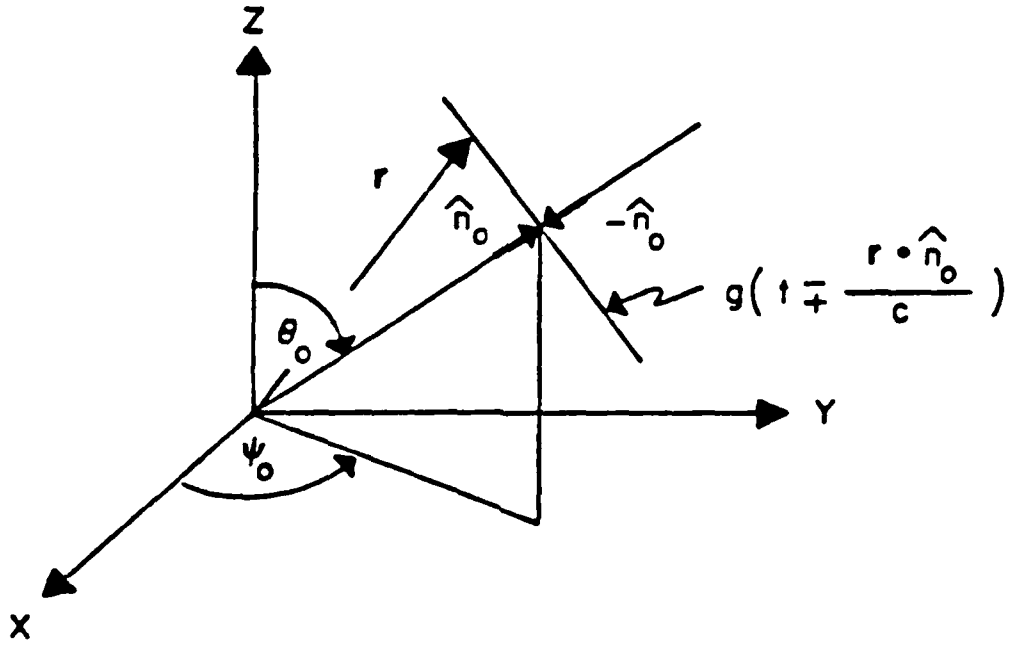


**Figure 2.2. General Plane-Wave Field $g\left(t \mp \frac{r \cdot \hat{n}_0}{c}\right)$ Propagating in the $\pm\hat{n}_0$ direction.**

The dimensionless direction cosines, $u_0$ and $v_0$, are given by

$$u_0 = \sin\theta_0 \cos\psi_0 \tag{2.13}$$

$$v_0 = \sin\theta_0 \sin\psi_0 \tag{2.14}$$

where $\theta_0$ is the depression angle and $\psi_0$ is the bearing angle. These angles are not known a priori.

If we consider multiple plane waves incident upon the planar array, equation (2.10) can be generalized and the deterministic part of the output electrical signal at time instant $\ell$ and element $(m,n)$ is

$$y(\ell,m,n) = \sum_k g_k \left( \ell T_S \stackrel{-}{+} \frac{u_{0k} m d_X + v_{0k} n d_Y}{c} \right) \tag{2.15}$$

where $g_k(t)$, $u_{0k}$, and $v_{0k}$ are the arbitrary baseband function and direction cosines associated with the $k$th sound source.

A brief description of the development of the frequency domain adaptive beamforming algorithm is presented next. The discussion that follows is based, in part, on the material in Ref. 7.

Define the complex estimation error at harmonic $q$ as

$$e(q) \stackrel{\Delta}{=} s(q) - \hat{s}(q). \tag{2.16}$$

The reference signal $s(q)$ is defined as

$$s(q) = \frac{1}{LMN} \sum_{m=-M'}^{M'} \sum_{n=-N'}^{N'} |R(q,m,n)| \exp\left[+j \angle R(q,0,0)\right] \tag{2.17}$$

and

$$\begin{aligned} \hat{s}(q) &= \frac{1}{LMN} \sum_{m=-M'}^{M'} \sum_{n=-N'}^{N'} c(q,m) d(q,n) R(q,m,n) \\ &= \underline{c}^T(q) \underline{\underline{R}}(q) \underline{d}(q) / (LMN) \end{aligned} \tag{2.18}$$

is the estimate of $s(q)$, where $c(q,m)$ and $d(q,n)$ are the unit magnitude complex weights in the $X$ and $Y$ directions, respectively, $\underline{c}(q)$ and $\underline{d}(q)$ are the $M \times 1$ and $N \times 1$ complex weight vectors in the $X$ and $Y$ directions, respectively, which are given by

$$\underline{c}(q) = [c(q,-M'),\ldots,c(q,0),\ldots,c(q,M')]^T \tag{2.19}$$

and

$$\underline{d}(q) = [d(q,-N'),\ldots,d(q,0),\ldots,d(q,N')]^T, \tag{2.20}$$

and $\underline{R}(q)$ is the $M \times N$ complex data matrix given by

$$\underline{R}(q) = \begin{bmatrix} R(q,-M',-N') & \ldots & R(q,-M',0) & \ldots & R(q,-M',N') \\ \vdots & & \vdots & & \vdots \\ R(q,0,-N') & \ldots & R(q,0,0) & \ldots & R(q,0,N') \\ \vdots & & \vdots & & \vdots \\ R(q,M',-N') & \ldots & R(q,M',0) & \ldots & R(q,M',N') \end{bmatrix}. \tag{2.21}$$

Now define the $(M+N) \times 1$ complex weight vector $\underline{w}(q)$ as follows:

$$\underline{w}(q) \triangleq \left[\frac{\underline{c}(q)}{\underline{d}(q)}\right]. \tag{2.22}$$

We can obtain the original weight vector in the $X$ direction via

$$\underline{c}(q) = \underline{A}\ \underline{w}(q) \tag{2.23}$$

where

$$\underline{A} = \left[\underset{M \times M}{\underline{I}} \;\middle|\; \underset{M \times N}{\underline{0}}\right] \tag{2.24}$$

is a $M \times (M+N)$ matrix, $\underline{I}$ is a $M \times M$ identity matrix, and $\underline{0}$ is a $M \times N$ null matrix. Similarly, we can obtain the original weight vector in the $Y$ direction via

$$\underline{d}(q) = \underline{B}\ \underline{w}(q) \tag{2.25}$$

where

$$\underline{B} = \left[ \underset{N \times M}{\underline{0}} \;\middle|\; \underset{N \times N}{\underline{I}} \right] \tag{2.26}$$

is a $N \times (M+N)$ matrix, $\underline{0}$ is a $N \times M$ null matrix, and $\underline{I}$ is a $N \times N$ identity matrix as indicated.

Substituting equations (2.23) and (2.25) into equation (2.18) yields

$$\hat{s}(q) = \underline{w}^T(q)\underline{Z}(q)\underline{w}(q)/(LMN) \tag{2.27}$$

where

$$\underline{Z}(q) = \underline{A}^T\underline{R}(q)\underline{B} \tag{2.28}$$

is a $(M+N)\times(M+N)$ complex matrix. The complex weight vector that minimizes the mean-square error $E\{|e(q)|^2\}$ is given by [Ref. 5, Ref. 7]

$$\underline{w}_{i+1}(q) = \underline{w}_i(q) + 2\mu_i e_i(q)\left[\underline{Z}(q) + \underline{Z}^T(q)\right]^* \underline{w}_i^*(q), i = 0, 1, 2, \ldots \tag{2.29}$$

where

$$e_i(q) = s(q) - \hat{s}_i(q) \tag{2.30}$$

is the estimation error after the $i^{th}$ iteration,

$$\hat{s}_i(q) = \underline{w}_i^T(q)\underline{Z}(q)\underline{w}_i(q)/(LMN) \tag{2.31}$$

is the estimate of $s(q)$ after the $i^{th}$ iteration, and the step-size parameter $\mu_i$ is given by

$$\mu_i = \mu_0 = (\sigma_y^2 + \sigma_n^2)^{-1},\ i = 0, 1, 2, \ldots \tag{2.32}$$

where $\mu_0$ is a constant, and is equal to the inverse of the sum of the signal and noise power, $\sigma_y^2$ and $\sigma_n^2$, respectively, at the center element of the array. After each iteration of the algorithm, each component of the complex weight vector $\underline{w}_{i+1}(q)$ is normalized by its respective magnitude in order to maintain unit magnitude.

Once the complex weight vector, $\underline{w}_{i+1}(q)$, converges to a steady-state value, $\underline{w}_{ss}(q)$, the steady-state complex weight vectors $\underline{c}_{ss}(q)$ and $\underline{d}_{ss}(q)$ can be obtained from equations (2.23) and (2.25), respectively. The estimates of the depression and bearing angles at harmonic $q$, $\hat{\theta}_0(q)$ and $\hat{\psi}_0(q)$, respectively, are given by [Ref. 8: p. 175]

$$\hat{\theta}_0(q) = \sin^{-1}\left[\left\{\left[\hat{u}_0^{LS}(q)\right]^2 + \left[\hat{v}_0^{LS}(q)\right]^2\right\}^{1/2}\right], \quad q \neq 0 \tag{2.33}$$

and

$$\hat{\psi}_0(q) = \tan^{-1}\left[\hat{v}_0^{LS}(q)/\hat{u}_0^{LS}(q)\right], \quad q \neq 0 \tag{2.34}$$

where $\hat{u}_0^{LS}(q)$ and $\hat{v}_0^{LS}(q)$ represent estimates of the direction cosines obtained by using a least-squares fit to the "unwrapped" steady-state phase weights $\theta_{ss}^{u}(q,m)$ and $\theta_{ss}^{u}(q,n)$, respectively. In the absence of noise

$$\theta_{ss}^{u}(q,m) = \pm 2\pi q f_0 u_0(q) m d_X / c, \quad \begin{matrix} q = -L', \ldots, 0, \ldots L' \\ m = -M', \ldots, 0, \ldots M' \end{matrix} \tag{2.35}$$

and

$$\phi_{ss}^{u}(q,n) = \pm 2\pi q f_0 v_0(q) n d_Y / c, \quad \begin{matrix} q = -L', \ldots, 0, \ldots L' \\ n = -N', \ldots, 0, \ldots N' \end{matrix} \tag{2.36}$$

It should be noted that if $r(\ell,m,n)$, $y(\ell,m,n)$, and $n(\ell,m,n)$ of equation (2.1) are baseband complex envelopes, then $qf_0$ must be replaced by $(f_c + qf_0)$ in equations (2.35) and (2.36), where $f_c$ is the carrier frequency in hertz. In addition, equations (2.33) and (2.34) must now be evaluated at $q = 0$. Substitution of equations (2.17) and (2.18) into equation (2.16) yields the following expression for the steady-state estimation error

$$e_{ss}(q) = \frac{1}{LMN} \sum_{m=-M'}^{M'} \sum_{n=-N'}^{N'} |R(q,m,n)| \Big[ \exp[+j \angle R(q,0,0)] - \exp\{+j[\theta_{ss}^{w}(q,m) + \phi_{ss}^{w}(q,n) + \angle R(q,m,n)]\} \tag{2.37}$$

where

$$R(q,m,n) = |R(q,m,n)| \exp[+j \angle R(q,m,n)], \tag{2.38}$$

$$c_{ss}(q,m) = a_{ss}(q,m) \exp[+j\theta^{w}_{ss}(q,m)] = \exp\left[+j\theta^{w}_{ss}(q,m)\right], \tag{2.39}$$

and

$$d_{ss}(q,n) = b_{ss}(q,n) \exp[+j\phi^{w}_{ss}(q,n)] = \exp\left[+j\phi^{w}_{ss}(q,n)\right] \tag{2.40}$$

where $a_{ss}(q,m) = 1$ and $b_{ss}(q,n) = 1$ are real, unit magnitude, amplitude weights and $\theta^{w}_{ss}(q,m)$ and $\phi^{w}_{ss}(q,n)$ are real, "wrapped", phase weights.

To ensure obtaining the correct depression and bearing angle estimates, $\hat{\theta}_0(q)$ and $\hat{\psi}_0(q)$, respectively, the steady-state phase weights need to be "unwrapped." The "unwrapped" steady-state phase weights can take on values outside the closed interval $[-\pi, \pi]$ and therefore ensures full angular coverage capability (i.e., $0 \leq \theta_0(q) \leq \pi/2$ and $0 \leq \psi_0(q) \leq 2\pi$). The use of "wrapped" phase weights is necessitated by computer programming limitations.

The question now arises how to obtain the "unwrapped" steady-state phase weights in order to obtain least-squares estimates of the direction cosines at each harmonic. The first step is to force the "wrapped" steady-state phase weights, $\theta^{w}_{ss}(q,m)$ and $\phi^{w}_{ss}(q,n)$, to be equal to zero at the center of the planar array (i.e., $m = 0, n = 0$). This is accomplished by multiplying each component of $\underline{c}_{ss}(q)$ and $\underline{d}_{ss}(q)$ (equations (2.19) and (2.20)) by $\exp[-j\theta^{w}_{ss}(q,0)]$ and $\exp[-j\phi^{w}_{ss}(q,0)]$, respectively.

The next step is to obtain rough estimates of the direction cosines, $u_0(q)$ and $v_o(q)$. The "wrapped" steady-state phase weight, $\theta^{w}_{ss}(q,m)$, can be expressed as

$$\theta_{ss}^{w}(q,m) \approx \pm\left[2\pi q f_o u_o(q) m d_x/c\right] + 2i\pi, \quad \begin{array}{l} i = 0, \pm 1, \pm 2, \ldots \\ q = -L', \ldots, 0, \ldots, L' \\ m = -M', \ldots, 0, \ldots, M' \end{array} \tag{2.41}$$

where $i$ is chosen to ensure that the value of $\theta_{ss}^{w}(q,m)$ is within the interval $[-\pi, \pi]$. In the computer simulations presented in this thesis, the interelement spacing is

$$d_x = d_y = \lambda_{min}/2 \tag{2.42}$$

where the minimum wavelength is

$$\lambda_{min} = c/f_{max} \tag{2.43}$$

and

$$f_{max} = L' f_o \text{ Hz.} \tag{2.44}$$

Substituting equations (2.43) and (2.44) into equation (2.42) yields

$$d_x = d_y = c/(2L' f_o) \tag{2.45}$$

where $L'$ is defined by equation (2.2) and $f_o$ is defined by equation (2.6). Substituting equation (2.45) into equation (2.41) yields

$$\theta_{ss}^{w}(q,m) \approx \pm(q/L') m u_o(q)\pi + 2i\pi, \quad \begin{array}{l} i = 0, \pm 1, \pm 2, \ldots \\ m = -M', \ldots, 0, \ldots, M' \\ q = -L', \ldots, 0, \ldots, L'. \end{array} \tag{2.46}$$

By letting $i = 0$ in equation (2.46), the following rough estimate of direction cosine $u_o$ at harmonic $q$ and element $m$ is obtained:

$$\hat{u}_o(q,m) = \pm\frac{L'}{qm\pi}\theta^w_{ss}(q,m), \quad q \neq 0, \quad m = \pm 1. \tag{2.47}$$

For purposes of this thesis, the rough estimates of $u_o(q)$ used were obtained by averaging the results obtained by evaluating equation (2.47) at elements $m = \pm 1$, that is,

$$\hat{u}_o(q) = 0.5\left[\hat{u}_o(q,1) + \hat{u}_o(q,-1)\right], \quad q \neq 0. \tag{2.48}$$

The most difficult case for the algorithm is to locate the highest harmonic, that is, $q = \pm L'$, when it exists at endfire ($\theta_o = 90°$) relative to the planar array. Let us assume that the value of the direction cosine at the highest harmonic is equal to one. Therefore, if $q = +L'$, equation (2.46) reduces to

$$\theta^w_{ss}(L',m) = m\pi + 2i\pi, \qquad \begin{matrix} i = 0, \pm 1, \pm 2, \ldots \\ m = -M', \ldots, 0, \ldots, M' \end{matrix} \tag{2.49}$$

Evaluating this relationship at element $m = \pm 1$ to obtain the rough estimate of $u_o(q)$ yields

$$\theta^w_{ss}(L', \pm 1) = \pm\pi + 2i\pi, \qquad i = 0, \pm 1, \pm 2, \ldots, \tag{2.50}$$

and since the "wrapped" steady-state value must be in the interval $[-\pi, \pi]$, $i$ must be equal to zero. Equation (2.50) is reduced to

$$\theta^w_{ss}(L', \pm 1) = \pm\pi. \tag{2.51}$$

If the plus sign is chosen in equation (2.47), and $m = \pm 1$ and $q = L'$, then evaluation of equation (2.47) yields

$$\hat{u}_o(L', \pm 1) = \theta^w_{ss}(L', \pm 1)/\pm\pi). \tag{2.52}$$

Upon substituting equation (2.51) into equation (2.52) we obtain

$$\hat{u}_o(L', \pm 1) = 1 \tag{2.53}$$

which is the expected result in the absence of noise since the assumption was made that the value of the direction cosine was equal to one at the highest harmonic. Evaluating equation (2.49) at a different element (i.e., $m \neq \pm 1$) would yield $i \neq 0$ and, as a result, an incorrect rough estimate of $u_0(L') = 1$. This validates the use of elements $m = \pm 1$ to obtain the estimate of the direction cosines (equation (2.47)).

The third step is to generate rough estimates of the "unwrapped" steady-state phase weights, $\hat{\theta}^u_{ss}(q,m)$, by replacing $u_o(q)$ in equation (2.46) with $\hat{u}_o(q)$ from equation (2.48), that is

$$\hat{\theta}^u_{ss}(q,m) = \pm(q/L')m\hat{u}_o(q)\pi, \quad \begin{matrix} q = -L', \ldots, 0, \ldots, L' \\ m = -M', \ldots, 0, \ldots, M' \end{matrix} \tag{2.54}$$

Therefore, if

$$i\pi < \left|\hat{\theta}^u_{ss}(q,m)\right| \leq (i+2)\pi, \quad \begin{matrix} i = 1,3,5,\ldots \\ q = -L', \ldots, 0, \ldots, L' \\ m = -M', \ldots, 0, \ldots, M' \end{matrix} \tag{2.55}$$

then

$$\theta^u_{ss}(q,m) = \theta^w_{ss}(q,m) + sgn\left[\hat{\theta}^u_{ss}(q,m)\right](i+1)\pi, \quad \begin{matrix} i = 1,3,5,\ldots \\ q = -L', \ldots, 0, \ldots, L' \\ m = -M', \ldots, 0, \ldots, M' \end{matrix} \tag{2.56}$$

where $sgn[\ ]$ is the sign function. Note that the right-hand side of equation (2.56) is simply the noise corrupted version of the right-hand side of equation (2.35).

The method of least-squares is then used to fit a straight line to the unwrapped phase weights $\theta^u_{ss}(q,m)$ as a function of element number $m$ for each harmonic $q$. The phase weights $\theta^u_{ss}(q,m)$ were computed using equation (2.56). The least-squares slope at harmonic $q$ is given by

$$\hat{s}_{LS}(q) = \sum_{m=-M;}^{M'} m\theta^u_{ss}(q,m) / \sum_{m=-M'}^{M'} m^2. \tag{2.57}$$

Substituting equation (2.45) into equation (2.35) yields

$$\theta^u_{ss}(q,m) = \pm(q/L')\pi u_o(q)m, \quad \begin{matrix} q = -L', \ldots, 0, \ldots, L' \\ m = -M', \ldots, 0, \ldots, M' \end{matrix} \tag{2.58}$$

in the absence of noise. Therefore, since in the presence of noise

$$\theta^u_{ss}(q,m) \approx \hat{s}_{LS}(q)m + \hat{b}_{LS}(q), \begin{matrix} q = -L', \ldots, 0, \ldots, L' \\ m = -M', \ldots, 0, \ldots, M' \end{matrix} \tag{2.59}$$

where

$$\hat{b}_{LS}(q) = \frac{1}{M} \sum_{m=-M'}^{M'} \theta^u_{SS}(q,m) \tag{2.60}$$

is the least-squares "$y$ intercept" at harmonic $q$, comparing equations (2.58) and (2.59) yields

$$\pm\hat{u}^{LS}_o(q) = [L'/(q\pi)]\,\hat{s}_{LS}(q), \quad q \neq 0 \tag{2.61}$$

which is the least-squares estimate of direction cosine $u_o$ at harmonic $q$.

In a similar derivation, it can be shown that the least-squares estimate of the direction cosine $v_o(q)$ at harmonic $q$ is given by

$$\pm\hat{v}^{LS}_o(q) = [L'/(q\pi)]\,\hat{s}_{LS}(q), \quad q \neq 0 \tag{2.62}$$

where now

$$\hat{s}_{LS}(q) = \sum_{n=-N'}^{N'} n\phi_{ss}^{u}(q,n) / \sum_{n=-N'}^{N'} n^2 \tag{2.63}$$

and, if

$$i\pi < \left|\hat{\phi}_{ss}^{u}(q,n)\right| \leq (i+2)\pi, \quad \begin{array}{l} i = 1,3,5,\ldots \\ q = -L',\ldots,0,\ldots,L' \\ n = -N',\ldots,0,\ldots,N' \end{array} \tag{2.64}$$

then

$$\phi_{ss}^{u}(q,n) = \phi_{ss}^{w}(q,n) + sgn\left[\hat{\phi}_{ss}^{u}(q,n)\right](i+1)\pi, \quad \begin{array}{l} i = 1,3,5,\ldots \\ q = -L',\ldots,0,\ldots,L' \\ n = -N',\ldots,0,\ldots,N' \end{array} \tag{2.65}$$

where

$$\hat{\phi}_{ss}^{u}(q,n) = \pm(q/L')n\hat{v}_o(q)\pi, \quad \begin{array}{l} q = -L',\ldots,0,\ldots,L' \\ n = -N',\ldots,0,\ldots,N' \end{array} \tag{2.66}$$

$$\hat{v}_o(q) = 0.5\left[\hat{v}_o(q,1) + \hat{v}_o(q,-1)\right], \quad q \neq 0 \tag{2.67}$$

and

$$\hat{v}_o(q,n) = \pm\frac{L'}{qn\pi}\phi_{ss}^{w}(q,n), \quad q \neq 0, \quad n = \pm 1. \tag{2.68}$$

Using the least-squares estimates of the direction cosines $\hat{u}_o^{LS}(q)$ and $\hat{v}_o^{LS}(q)$, that is, equations (2.61) and (2.62), respectively, yield estimates of the depression and bearing angles, $\hat{\theta}_o(q)$ and $\hat{\psi}_o(q)$, respectively, using equations (2.33) and (2.34).

# III. RESULTS

Significant computer simulation results from four unique test cases are presented in this chapter. The test cases were designed to test the algorithm's multiple broadband target localization capability, its full angular coverage capability, and its angular resolution as a function of the input SNR at a single element in the array, sampling rate, harmonic number, and the number of iterations.

The test cases were comprised of the following:

(1) Case 1 - a single broadband target located at broadside relative to the planar array;

(2) Case 2 - three broadband targets located at random positions;

(3) Case 3 - a single broadband target located at endfire relative to the planar array; and

(4) Case 4 - three broadband targets, two of which share a common harmonic.

The simulation results of these four test cases are based upon processing the output electrical signals from a $7 \times 7$ planar array of equally spaced hydrophones. The acoustic field incident upon the planar array was, in general, the sum of several plane-wave fields travelling in different directions. Each plane-wave field consisted of an arbitrary number of harmonics (spectral lines) emanating from one of the broadband sound sources. As a result, the output electrical signal at each element of the planar array was composed of an arbitrary number $K$ of harmonics, all with identical amplitudes of unity.

The fundamental frequency for all test cases was chosen to be $f_o = 1000$ Hz. Via equation (2.6), the fundamental period at each element of the array was 1 millisecond. The sampling parameter, $S$, was set equal to 2, 4, and 6, which

corresponded to a sampling frequency equal to the Nyquist Rate, twice the Nyquist Rate, and three times the Nyquist Rate, respectively. The number of time samples taken per element of the array is given by

$$L = SK + 1 \tag{3.1}$$

where $L$ is the total number of samples taken per element, $K$ is the total number of harmonics present in the signal, and $S$ is the sampling parameter.

Baseline, or "no noise" test case results, were the first generated to ensure that the algorithm was working properly in a noise-free environment. Figure 3.1 depicts the noise free, time domain, received signal for case 2. For each baseline test case, and for a given value of the sampling parameter, bearing and depression angle estimation errors (measured in degrees) were obtained by running the computer simulation once and allowing the modified complex LMS algorithm 100 iterations. Case 1 baseline test case results showed zero degree estimation errors whereas case 2 and case 3 baseline results showed estimation errors of less than 0.1 degrees. Case 4 baseline results will be discussed later in this chapter.

Following compilation of the baseline results, identical test cases were run using additive, wide-sense stationary, zero mean, white, guassian noise samples to corrupt the time samples of the received signal. Figure 3.2 depicts the time domain, received signal for case 2 for a $SNR = 0$ dB. For each test case, and for a given value of the sampling parameter and input $SNR$ at a single element of the array, average bearing and depression angle estimation errors were obtained by running the computer simulation 100 times per $SNR$ value and allowing the complex LMS algorithm 100 iterations per run. In all test cases, allowing the adaptive algorithm more than 100 iterations did not decrease the estimation errors.

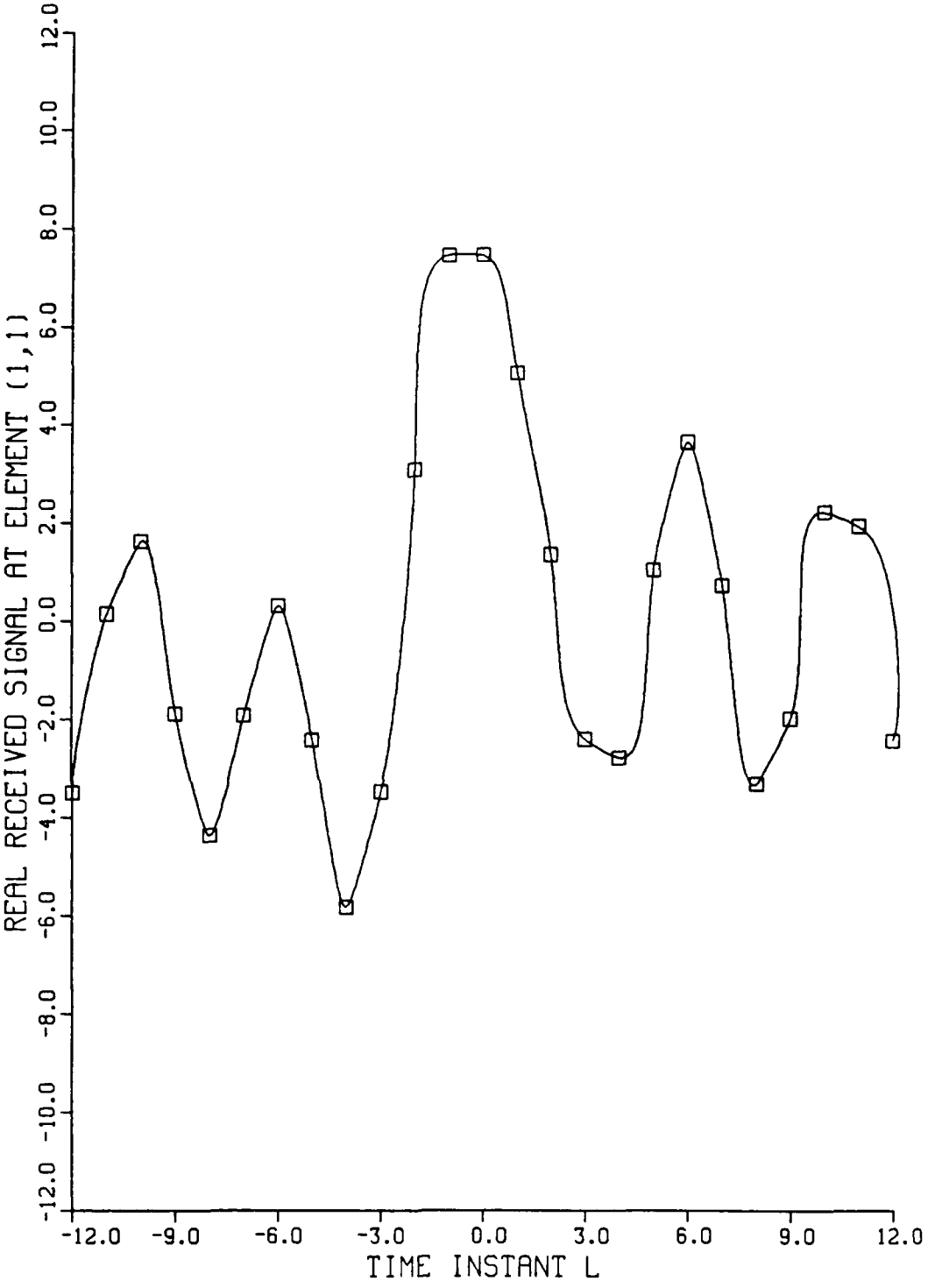


**Figure 3.1. Real Received Signal at Element (1,1), for Case 2 with No Noise Present.**

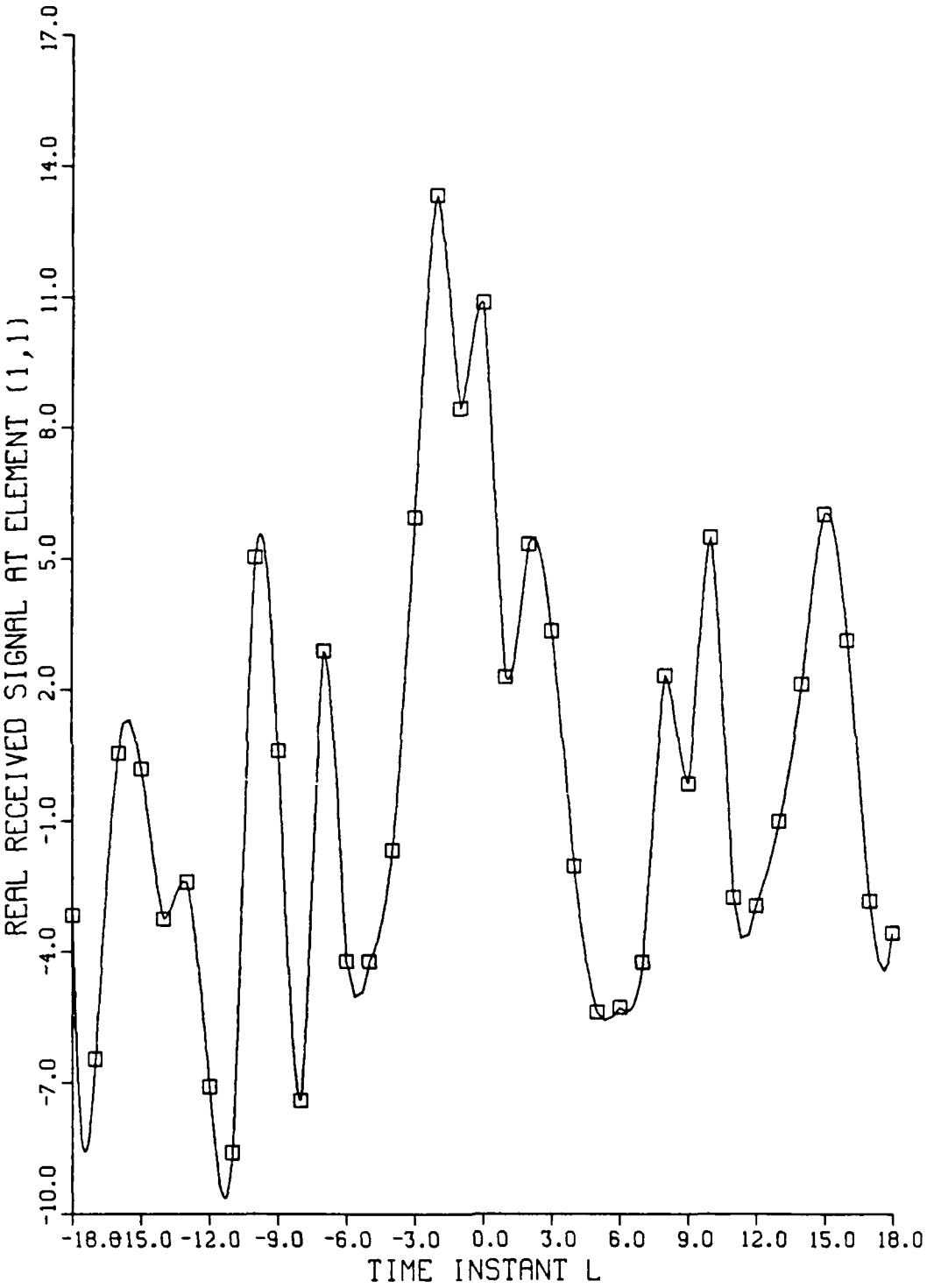


**Figure 3.2. Real Received Signal at Element (1,1) for Case 2 for $SNR = 0$ dB.**

Case 1 placed a single target at broadside relative to the planar array ( i.e., $\theta_o = 0°$). This was considered the simplest case for the algorithm since it is at broadside that the far-field beam pattern has its narrowest beamwidth and, as a result, the algorithm should provide good angular resolution [Ref. 8: pp. 62-66]. The general plane-wave field radiated by the target consisted of $K = 6$ harmonics. Therefore, with $K = 6$ and $S = 2, 4$, and 6, only $L = 13$, 25, and 37 time samples, respectively, were taken per element in the array (equation (3.1)). Figure 3.3 presents the average estimation error of the depression angle versus the sampling parameter $S$ for the 0 dB $SNR$ case. It can be seen that as the value of $S$ increases for a given harmonic, the magnitude of the estimation error decreases. If $S$ is held constant, it can be seen that as the harmonic number ($q$) increases, the magnitude of the estimation error decreases. These two trends were expected. As the value of $S$ increases, more time samples are being processed and, as a result, the noise component of the received signal should tend to average out to be zero. Since more data is available for evaluation, a better estimate of the deterministic signal results. An increase in the harmonic number, $q$, represents an increase in the frequency and, as a result, the beamwidth of the far-field beam pattern decreases [Ref. 8: pp. 58-62]. The decreased beamwidth increases the angular resolution of the algorithm and, as a result, decreases the estimation error.

Figure 3.4 presents the results for case 1 at 9 dB $SNR$. The trends which were present in the 0 dB case are again apparent here. It also should be noted that as the $SNR$ value increases (i.e., from 0 dB to 9 dB), the magnitude of the estimation error decreases.

Results for bearing angle estimation error in the broadside case are irrelevant since the target is directly above the array, and the bearing angle has no meaning.

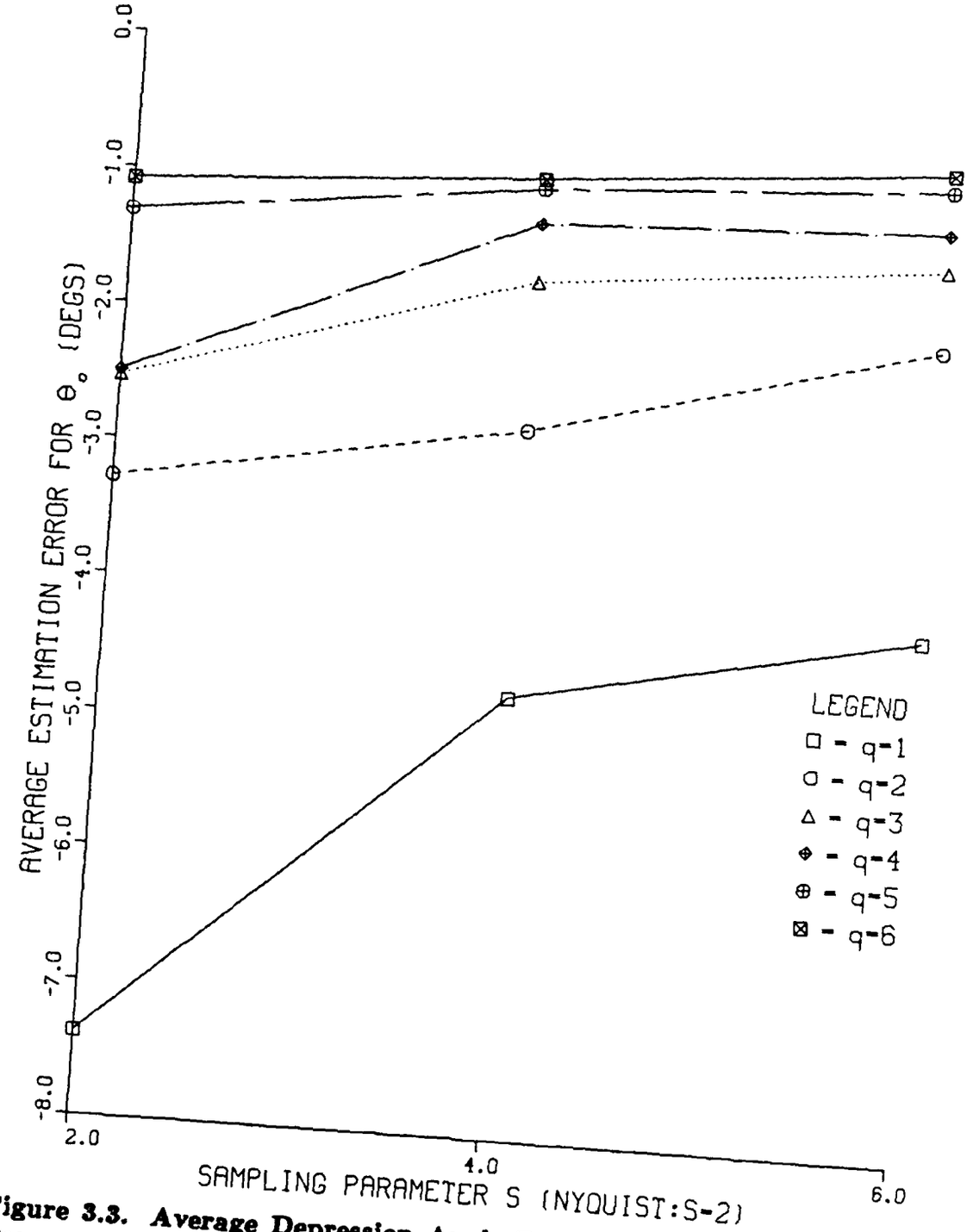


**Figure 3.3. Average Depression Angle Estimation Error vs Sampling Parameter $S$, Case 1: $SNR = 0$ dB. $I = 100$.**

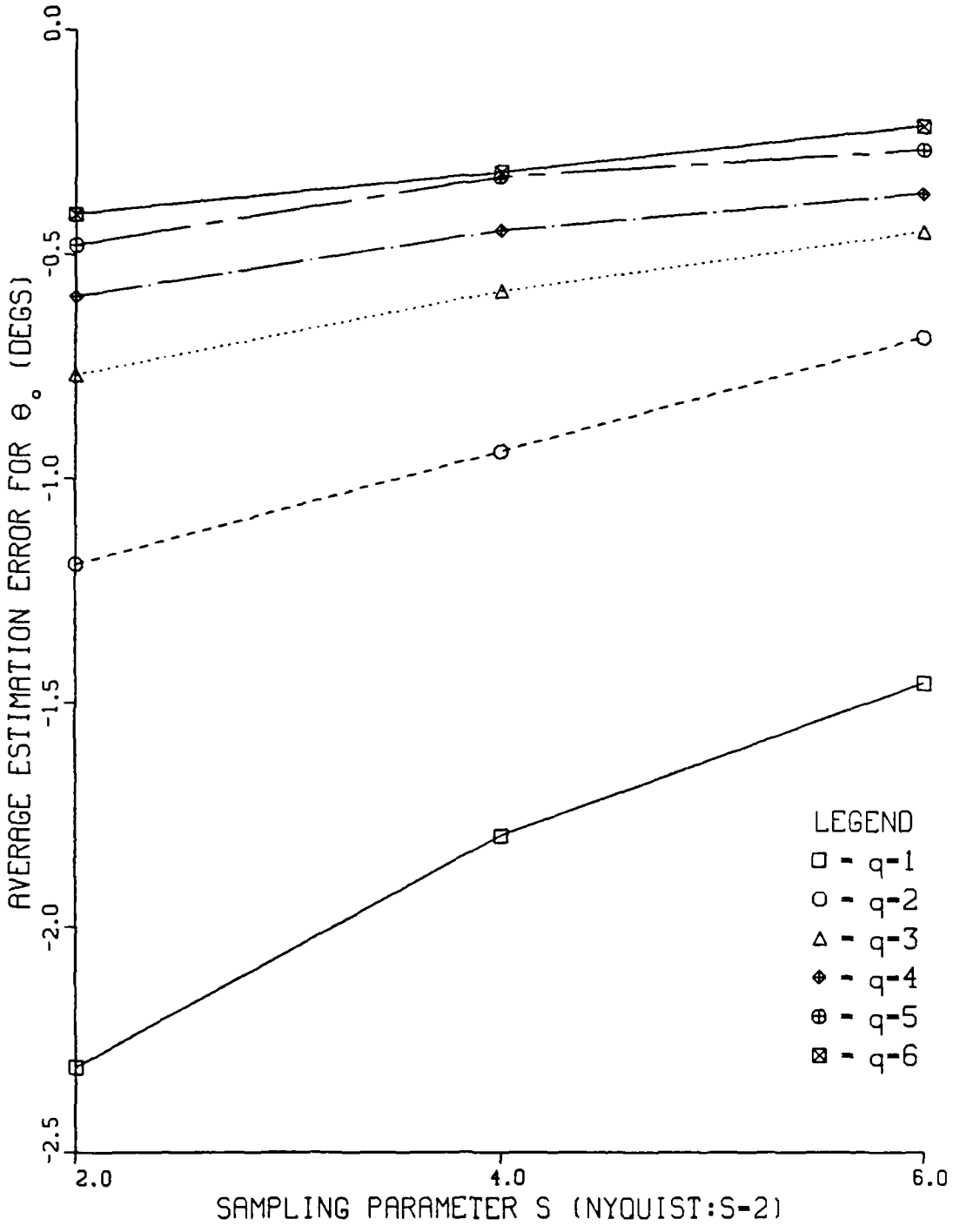


**Figure 3.4. Average Depression Angle Estimation Error vs Sampling Parameter $S$, Case 1: $SNR = 9$ dB. $I = 100$.**

Case 2 placed three broadband targets at random locations. The general plane-wave field radiated by each of the targets contained two unique harmonics. Target 1 was located at $(\theta_o = 49°, \psi_o = 38°)$ and radiated harmonics 1 and 6. Target 2 was located at $(\theta_o = 5, \psi_o = 137°)$ and radiated harmonics 2 and 5. Target 3 was located at $(\theta_o = 77°, \psi_o = 307°)$ and radiated harmonics 3 and 4. Since there are three incident plane-wave fields each containing two unique harmonics, the output electrical signal from each element in the array exhibits a total of $K = 6$ harmonics. As before, equation (3.1) dictates that only $L = 13, 25$, and 37 time samples are to be taken per element of the array when $S = 2, 4$, and 6, respectively. Figure 3.5 presents case 2 results for the depression angle estimation error with a 0 dB $SNR$. In general, as $S$ increases, the estimation error decreases for a given harmonic. When comparing the harmonics associated with a particular target, the highest harmonic usually is associated with the lessor of the estimation errors. These general results can be explained using the same arguments presented for case 1.

Figure 3.6 presents the case 2 bearing angle estimation errors for 0 dB $SNR$. Figures 3.7 and 3.8 present the case 2 estimation errors for the depression and bearing angle, respectively, for 9 dB $SNR$. The same general trends already introduced are apparent in Figures 3.5 through 3.8. As in case 1, as the $SNR$ value increased, the magnitude of the estimation errors decreased.

Case 3 placed a single broadband target at endfire relative to the planar array $(\theta_o = 90°, \psi_o = 90°)$. This case was considered the most difficult for the algorithm since it is at endfire that the far-field beam pattern beamwidth is its broadest [Ref. 8: pp. 62-66]. The general plane-wave field radiated by the target consisted of $q = 5$ harmonics. Therefore, with $S = 2, 4$, and 6, only $L = 11, 21$, and 31 time samples were taken, respectively, at each element of the array (equation (3.1)). Figures

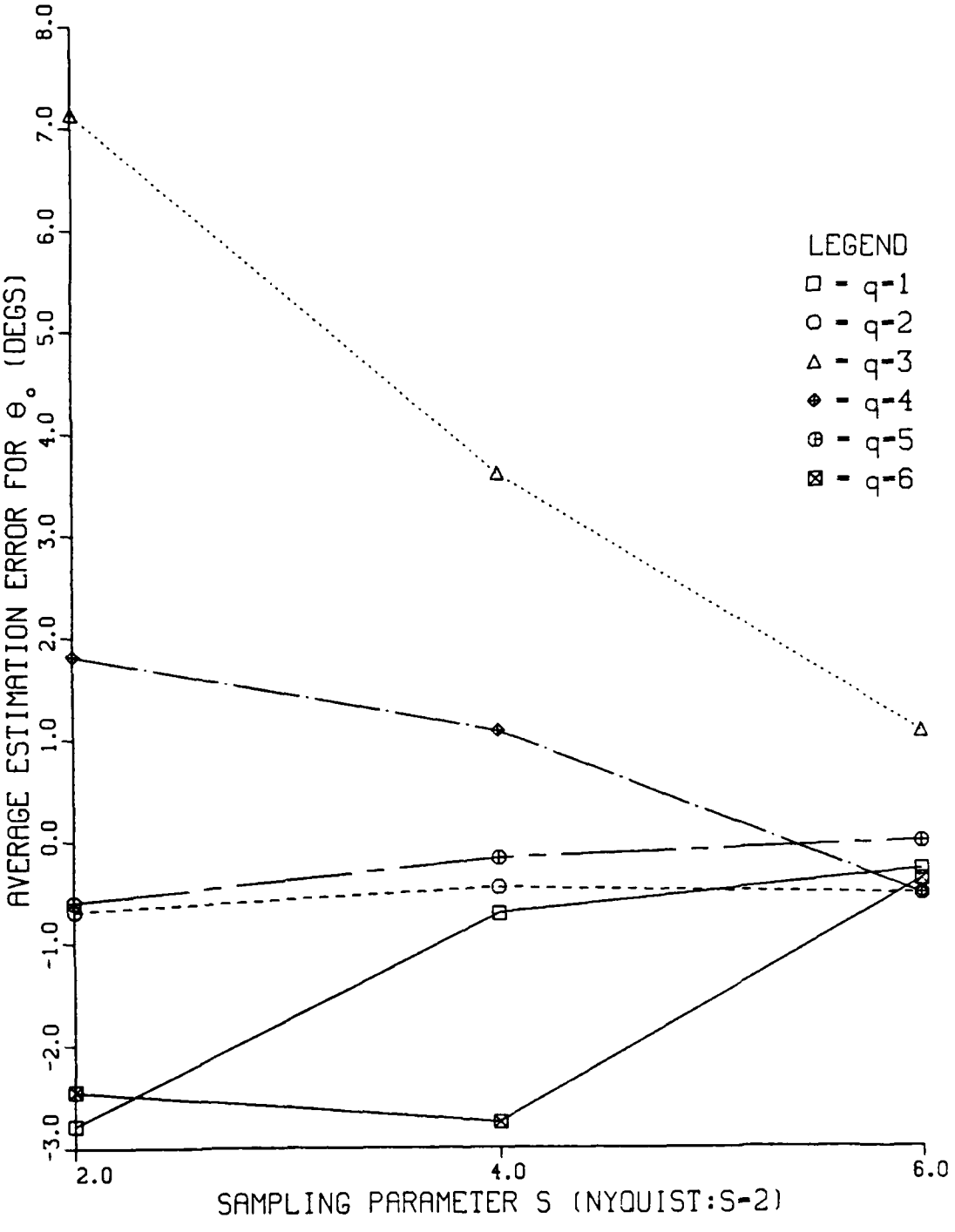


**Figure 3.5. Average Depression Angle Estimation Error vs Sampling Parameter $S$, Case 2: $SNR = 0$ Db. $I = 100$.**

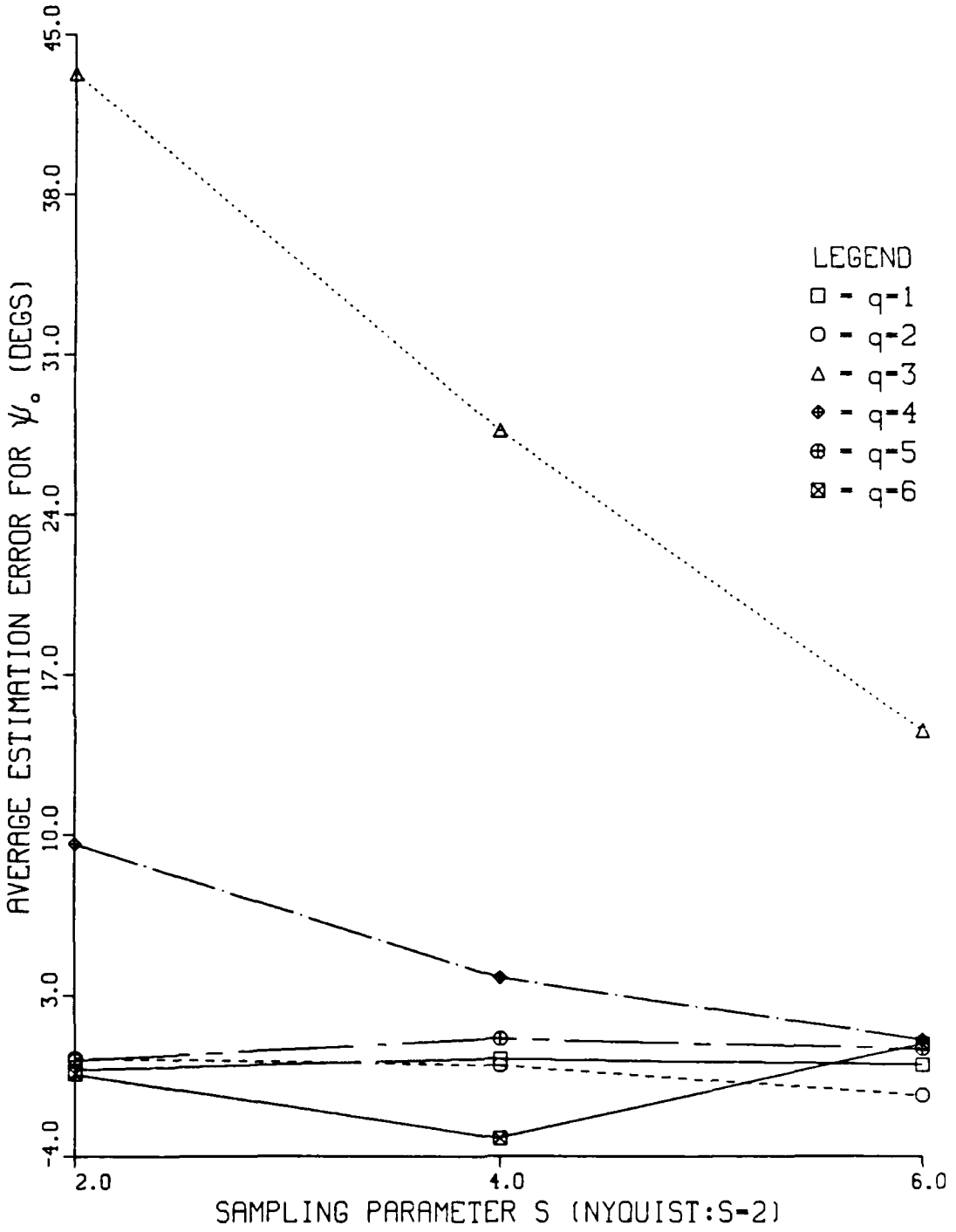


**Figure 3.6. Average Bearing Angle Estimation Error vs Sampling Parameter $S$, Case 2: $SNR = 0$ dB $I = 100$.**

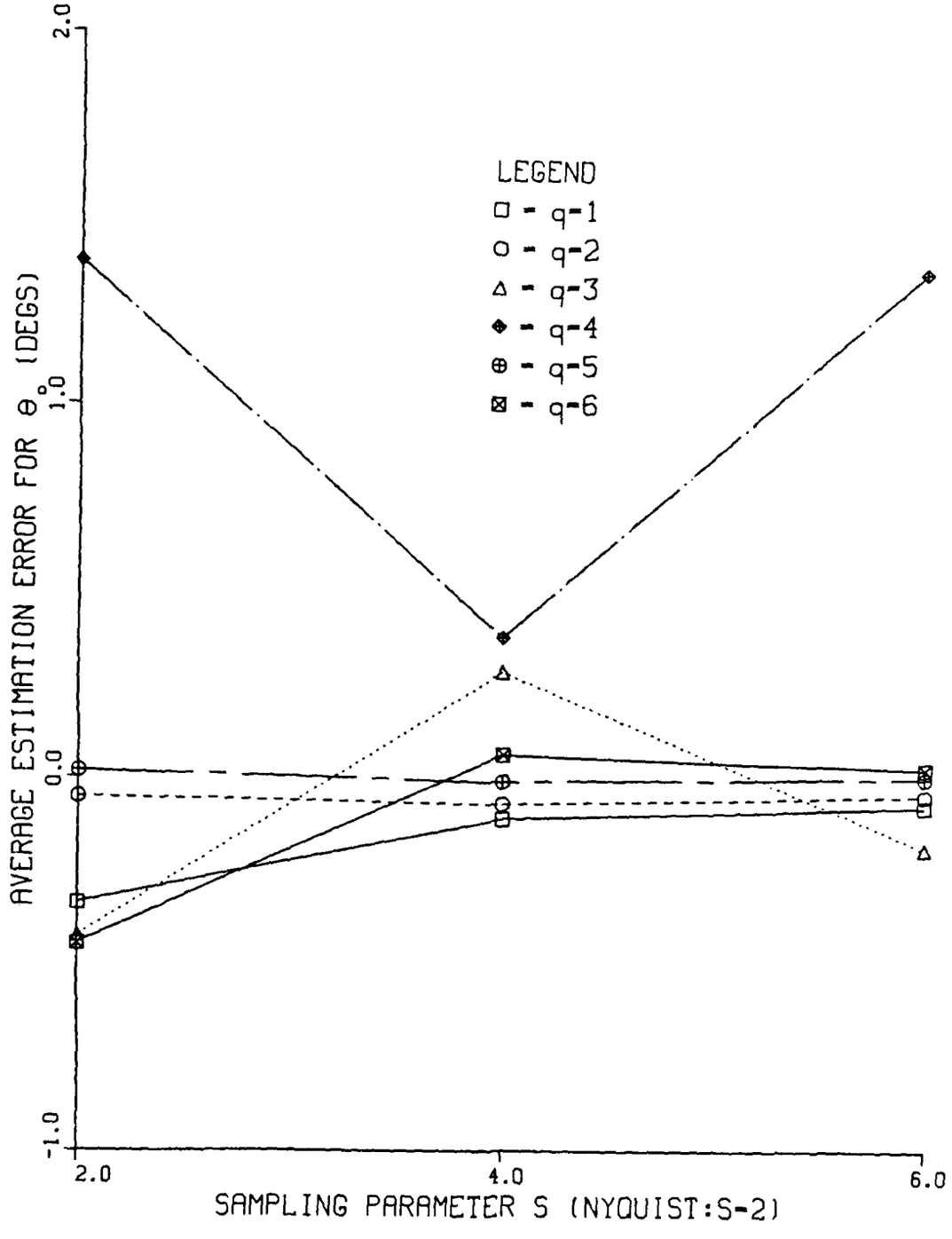


**Figure 3.7. Average Depression Angle Estimation Error vs Sampling Parameter $S$, Case 2: $SNR = 9$ dB $I = 100$.**

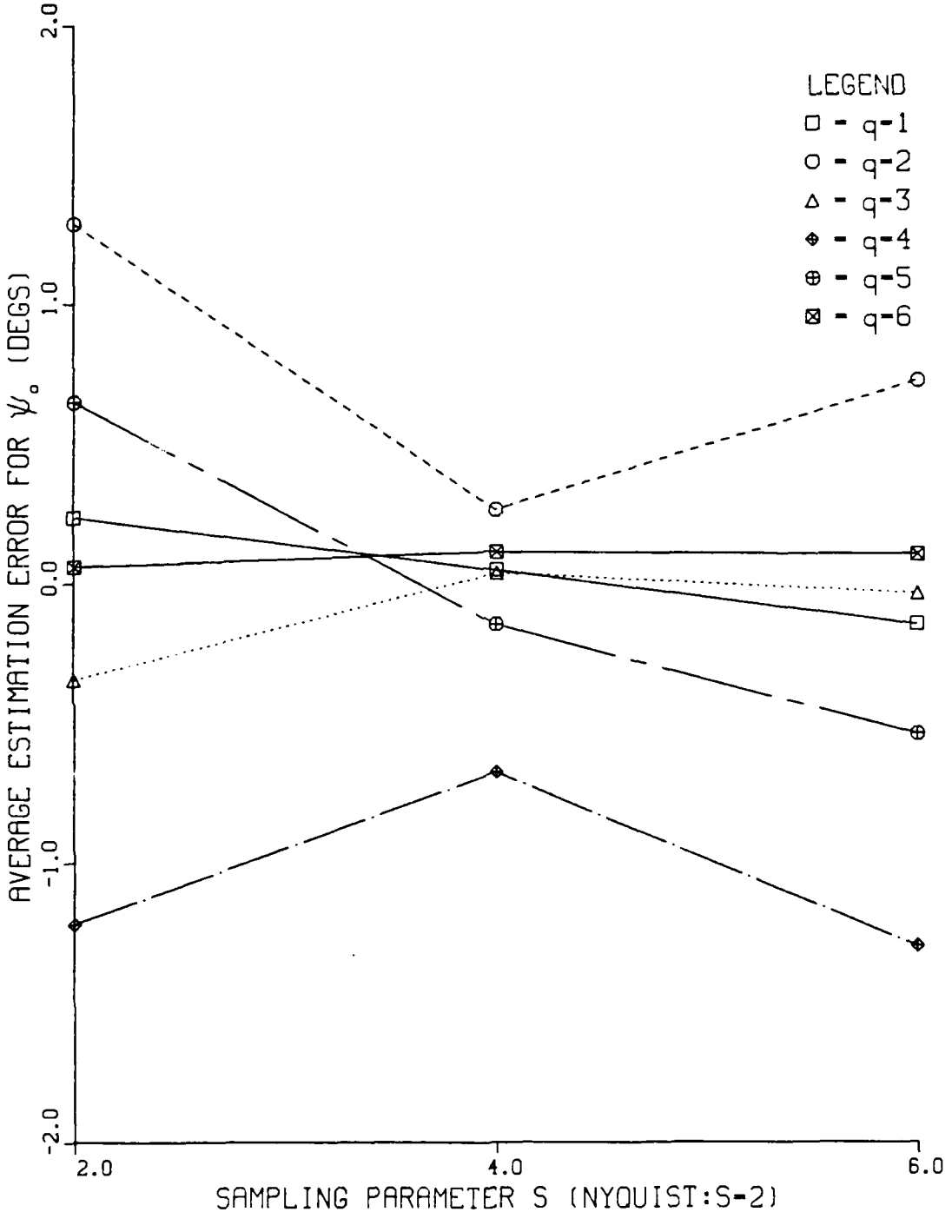


**Figure 3.8. Average Bearing Angle Estimation Error vs Sampling Parameter $S$, Case 2: $SNR = 9$ dB $I = 100$.**

3.9 and 3.10 illustrate the average depression and bearing angle estimation errors, respectively, for 0 dB $SNR$. Figures 3.11 and 3.12 illustrate the same information for 9 dB $SNR$. The estimation errors for the highest harmonic ($q = 5$) are not shown for any of the case 3 results since the magnitude of these errors was between 70 and 90 degrees. This poor performance for the highest harmonic at endfire can be explained theoretically (see Chapter 2 - phase unwrapping).

Case 4 corresponded to three broadband targets being present. The general plane-wave field radiated by each target was composed of two harmonics. In this case, two of the targets shared a common spectral line, namely, the fundamental frequency ($q = 1$). Target 1 was located at ($\theta_o = 45°, \psi_o = 0°$) and radiated harmonics 1 and 2. Target 2 was located at ($\theta_o = 45°, \psi_o = 180°$) and radiated harmonics 1 and 5. Target 3 was located at ($\theta_o = 33°, \psi_o = 47°$) and radiated harmonics 3 and 4. A total of $K = 5$ harmonics were present in the output electrical signals, and, with $S = 2, 4$, and 6; only $L = 11, 21$, and 31 time samples, respectively, were taken at each element of the array (equation (3.1)). For this case, only no noise results were compiled, with the computer simulation running once and the complex LMS adaptive algorithm allowed 100 iterations.

For harmonics $q = 2, 3, 4$, and 5 contained in the output electrical signal, the algorithm correctly identified the location of the targets with zero degrees estimation error. However, for the shared harmonic ($q = 1$), the algorithm located a false fourth target, which was located exactly between the actual locations of the targets whose radiated general plane-wave fields contained the shared harmonic, namely, targets 1 and 2.

Tabular numerical data for test cases 1 through 4 is contained in The Appendix.

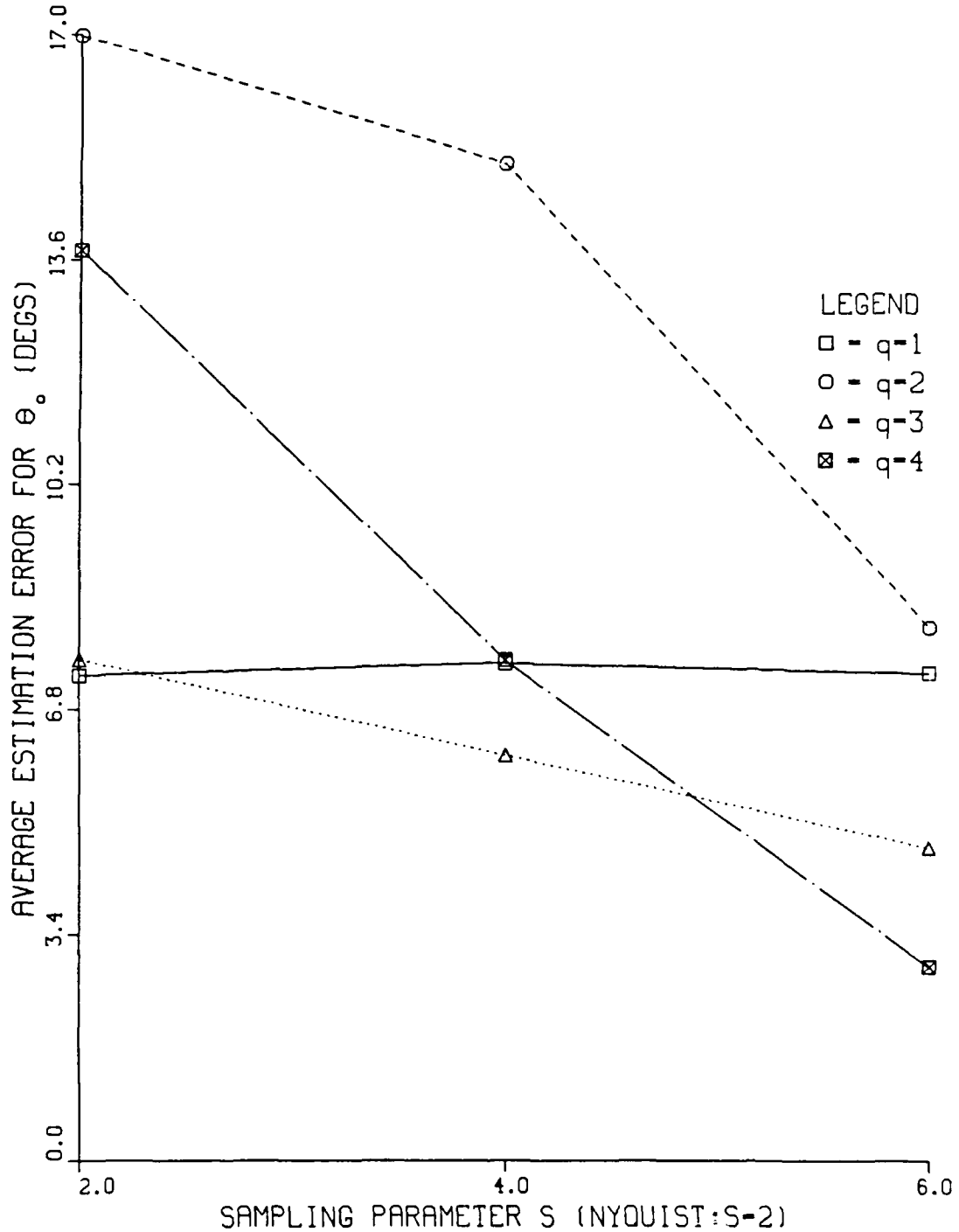


**Figure 3.9. Average Depression Angle Estimation Error vs Sampling Parameter $S$, Case 3: $SNR = 0$ dB $I = 100$.**

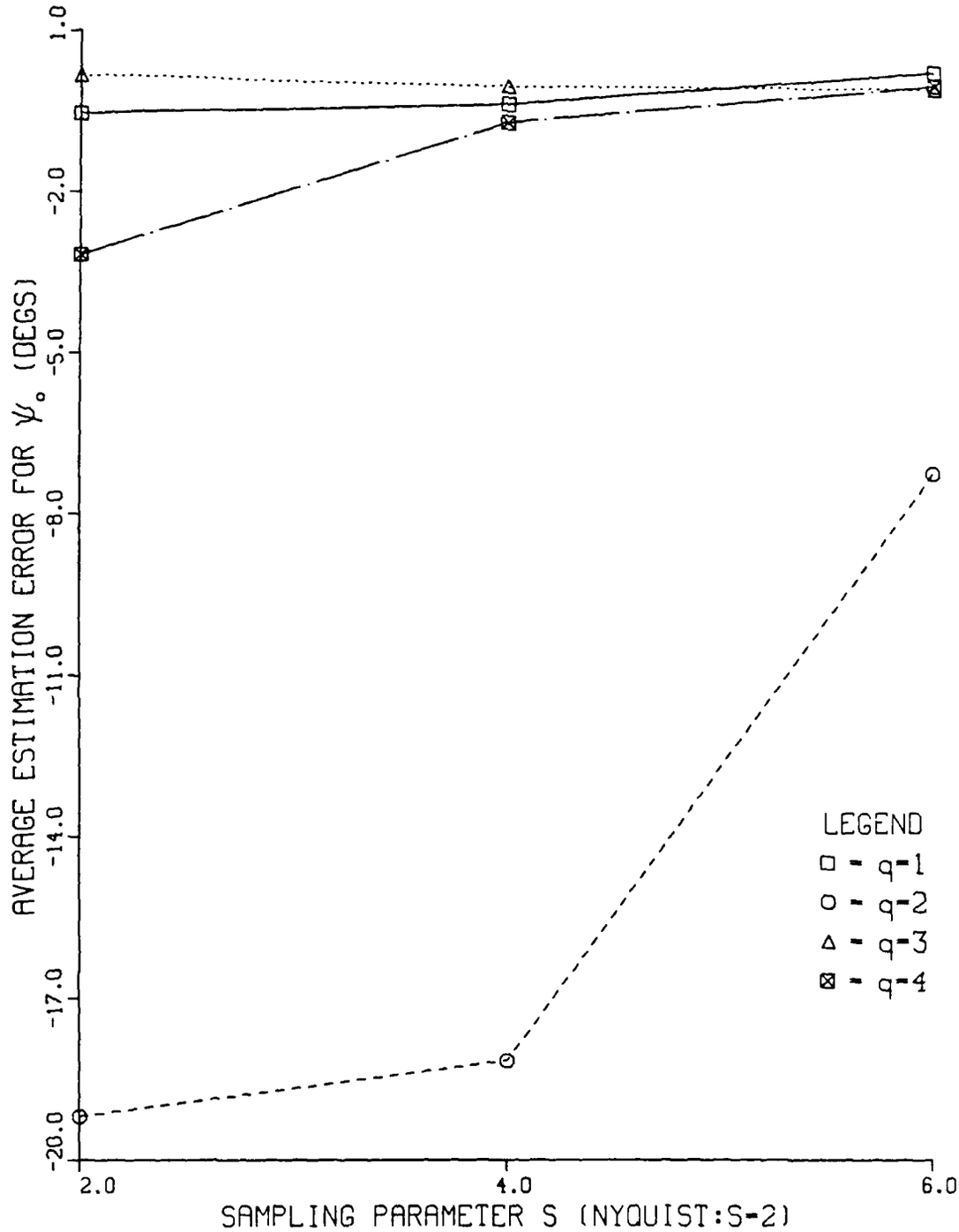


**Figure 3.10. Average Bearing Angle Estimation Error vs Sampling Parameter $S$, Case 3: $SNR = 0$ dB $I = 100$.**

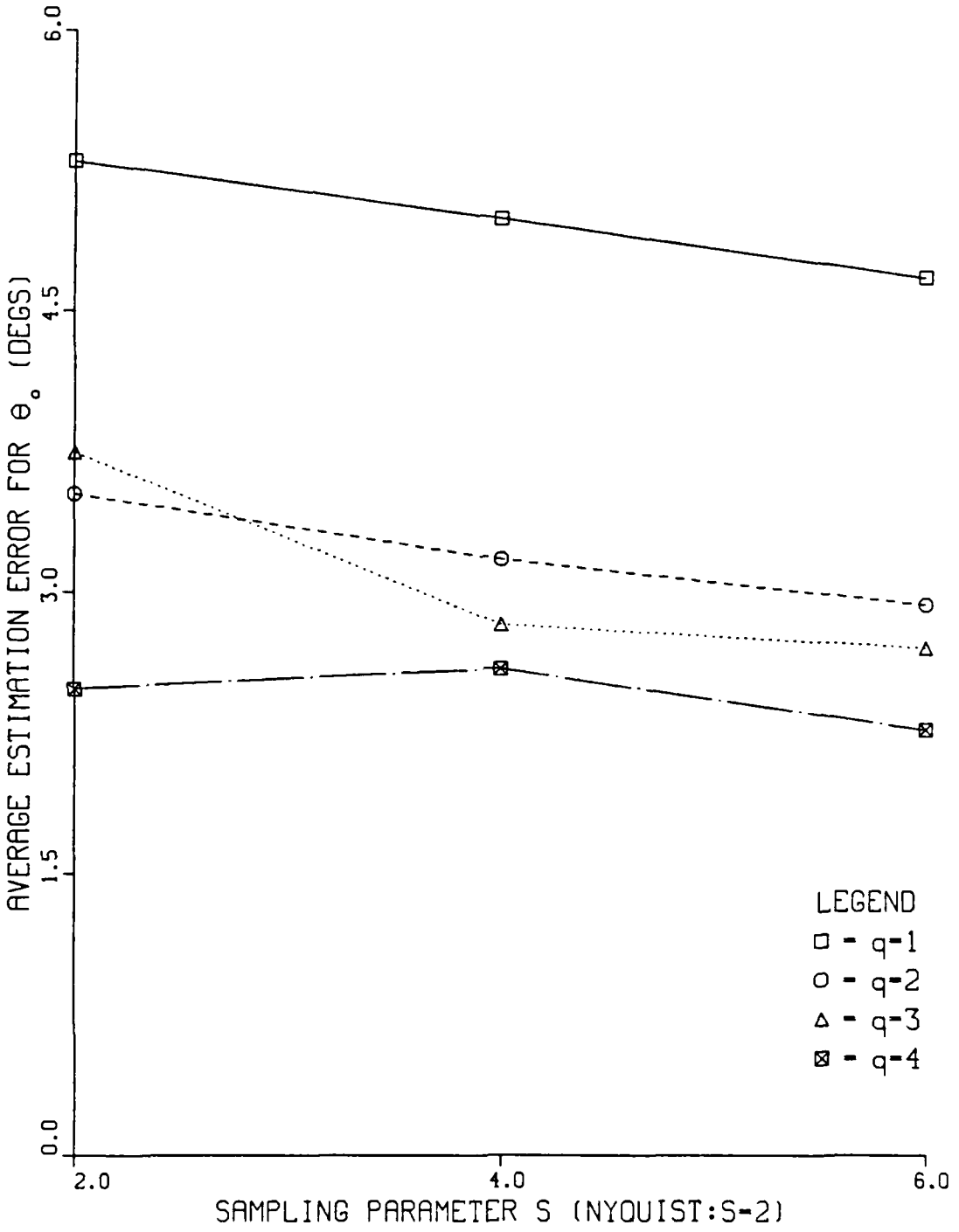


**Figure 3.11. Average Depression Angle Estimation Error vs Sampling Parameter $S$, Case 3: $SNR = 9$ dB $I = 100$.**

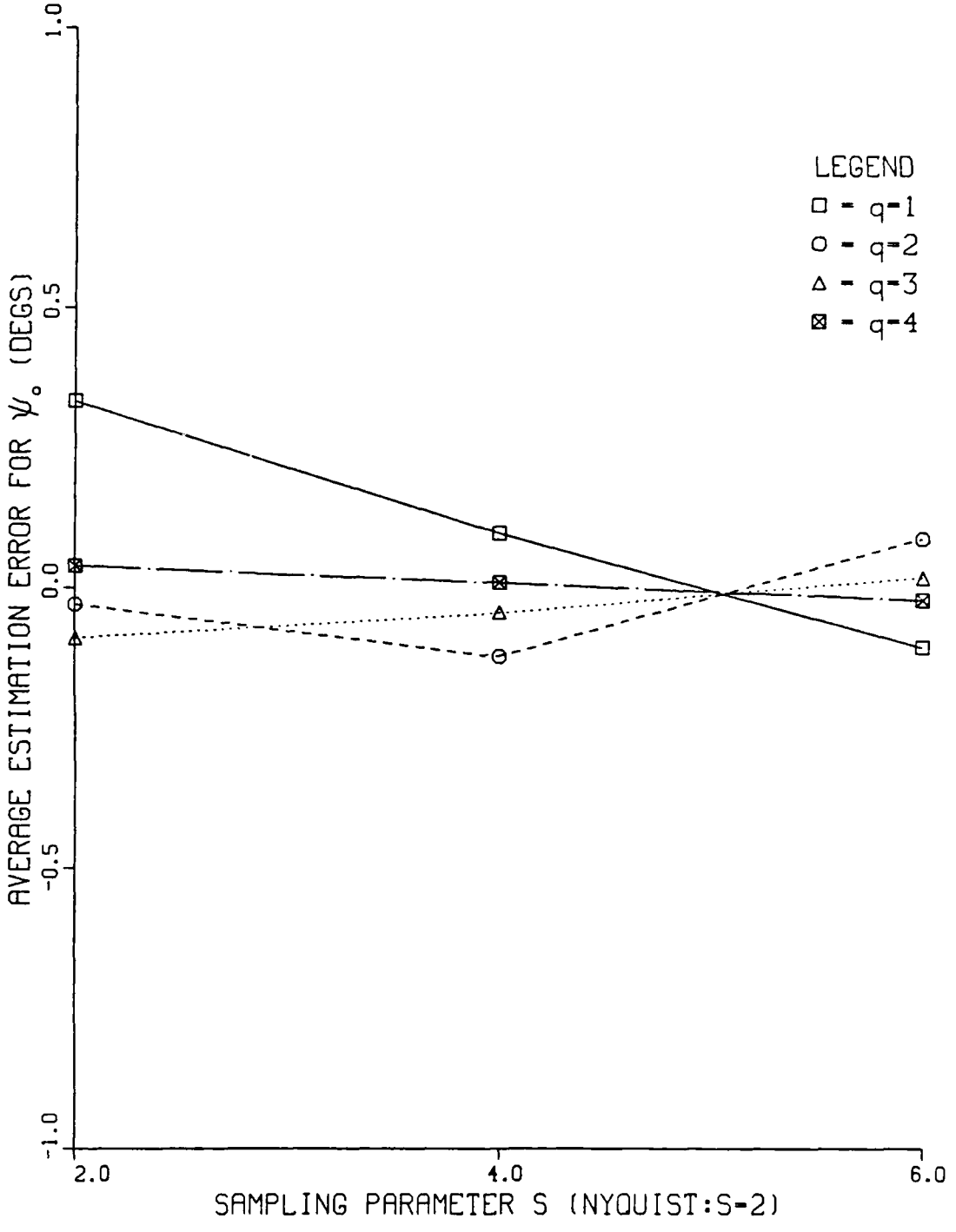


**Figure 3.12. Average Bearing Angle Estimation Error vs Sampling Parameter $S$, Case 3: $SNR = 9$ dB $I = 100$.**

test case 2 because it was felt that this case presented the most realistic real world situation. First, a minimum number of iterations for the algorithm to produce the same results as presented in this chapter (when 100 iterations of the algorithm was allowed) was found. The minimum number was found to be 10 iterations. Using this information, the step size parameter, $\mu$, (which had been a constant) was varied using a step function. For the first 10 iterations of the algorithm, $\mu$ was held constant. This allowed the algorithm to reach its minimum value with a constant $\mu$. The value for $\mu$ was then stepped down to one-tenth its original value for an additional 90 iterations. No decrease in estimation error resulted. The parameter was then stepped down to one one-hundredth, and then one one-thousandth, of its original value, with no change in the estimation error resulting. Additional attempts to model the step size parameter as a decreasing exponential yielded no change in the estimation error.

# IV. CONCLUSIONS AND RECOMMENDATIONS

The goal of this thesis was to evaluate a frequency domain adaptive beamforming algorithm which was developed by Ziomek and Chan [Ref. 5]. The multiple broadband target localization capability and the full angular coverage capability of the algorithm were of particular interest.

Chapter 3 presented the results of four test cases which were designed to test the algorithm for several different capabilities. Several conclusions concerning the performance of the frequency domain adaptive beamforming algorithm can be drawn from these results. Among these conclusions is the fact that the algorithm performs well in all test cases, yielding what would be considered acceptable estimation errors for the target localization problem. It should also be noted here that the number of time samples taken per element of the array never exceeded 37 time samples, an amount which represents a small number of data points.

The algorithm does exhibit multiple broadband target localization capability. The test case results show that multiple targets can be localized if their radiated acoustic plane-wave fields contain at least one unique spectral line. The separation distance of the spectral lines can be controlled by selecting an appropriate value for the FFT bin spacing. The algorithm has also demonstrated its ability to localize targets both at endfire and broadside positions relative to the planar array, thus demonstrating the algorithm's full angular coverage capability.

Several general trends were apparent in the results. The first of these trends is that as the sampling parameter $S$ increased, the magnitude of the estimation error decreased. This was due to a corresponding increase in the amount of time samples being processed. The second trend observed was that as the harmonic number $q$

increased, the magnitude of the estimation error, in general, decreased. This trend can be explained by the fact that as the harmonic number $q$ increases (equivalent to an increase in the frequency), the far-field beam pattern beamwidth decreases which results in better angular resolution. The third trend observed was that as the $SNR$ increased (the output electrical signal becoming less noisy), the magnitude of the estimation error decreased. It was also found that the estimation errors presented in this thesis are obtainable after ten iterations of the adaptive algorithm, and an increase in the number of iterations did not decrease the estimation error.

In the course of this investigation, several possible areas for future research presented themselves:

- further study of the effects of varying the step-size parameter, $\mu$, in an attempt to decrease the magnitude of the estimation error,
- investigation of a noise reduction system prior to processing the output electrical signals, and
- application of other spectral analysis techniques (i.e., autoregressive, maximum entropy, maximum likelihood, etc.) to produce frequency spectra.

# APPENDIX

The Appendix presents the tabular numerical data from which the graphical results of Chapter 3 were produced. The numerical data for the graphical results of Figures 3.3 through 3.12 is presented in Tables A.1 through A.10, respectively. Tables A.11 and A.12 presents the numerical data for Case 4. There is no corresponding graphical result for Case 4.

**TABLE A.1. NUMERICAL DATA CORRESPONDING TO FIGURE 3.3.**

Case 1: One target located at broadside relative to planar array; six harmonics present in output electrical signal; Sampling parameter S = 2, 4, and 6; 100 iterations; SNR = 0dB

| HARMONIC | LOCATION | | DEPRESSION ANGLE $\theta_\bullet$ ESTIMATION ERROR (DEG) | | |
|---|---|---|---|---|---|
| | $\theta_\bullet$ | $\psi_\bullet$ | | | |
| q | (DEG) | (DEG) | S=2 | S=4 | S=6 |
| 1 | 0 | 270 | -7.388 | -4.732 | -4.124 |
| 2 | 0 | 270 | -3.287 | -2.760 | -1.975 |
| 3 | 0 | 270 | -2.542 | -1.654 | -1.374 |
| 4 | 0 | 270 | -2.506 | -1.223 | -1.099 |
| 5 | 0 | 270 | -1.312 | -0.962 | -0.784 |
| 6 | 0 | 270 | -1.086 | -0.892 | -0.660 |

**TABLE A.2. NUMERICAL DATA CORRESPONDING TO FIGURE 3.4.**

Case 1: One target located at broadside relative to planar array; six harmonics present in output electrical signal; Sampling parameter S = 2, 4, and 6; 100 iterations; SNR = 9dB

| HARMONIC | LOCATION | | DEPRESSION ANGLE $\theta_0$ ESTIMATION ERROR (DEG) | | |
|---|---|---|---|---|---|
| | $\theta_0$ | $\psi_0$ | | | |
| q | (DEG) | (DEG) | S=2 | S=4 | S=6 |
| 1 | 0 | 270 | -2.312 | -1.796 | -1.456 |
| 2 | 0 | 270 | -1.191 | -0.940 | -0.686 |
| 3 | 0 | 270 | -0.769 | -0.582 | -0.449 |
| 4 | 0 | 270 | -0.594 | -0.446 | -0.365 |
| 5 | 0 | 270 | -0.479 | -0.326 | -0.267 |
| 6 | 0 | 270 | -0.410 | -0.316 | -0.214 |

**TABLE A.3. NUMERICAL DATA CORRESPONDING TO FIGURE 3.5.**

Case 2: Multiple targets located at random positions; six harmonics present in output electrical signal; Sampling parameter S = 2, 4, and 6; 100 iterations; SNR = 0dB

| HARMONIC | LOCATION | | DEPRESSION ANGLE $\theta_0$ ESTIMATION ERROR (DEG) | | |
|---|---|---|---|---|---|
| | $\theta_0$ | $\psi_0$ | | | |
| q | (DEG) | (DEG) | S=2 | S=4 | S=6 |
| 1 | 49 | 38 | -2.789 | -0.708 | -0.285 |
| 2 | 5 | 137 | -0.686 | -0.450 | -0.522 |
| 3 | 77 | 307 | +7.138 | +3.601 | +1.075 |
| 4 | 77 | 307 | +1.818 | +1.085 | -0.521 |
| 5 | 5 | 137 | -0.599 | -0.164 | -0.010 |
| 6 | 49 | 38 | -2.452 | -2.752 | -0.383 |

**TABLE A.4. NUMERICAL DATA CORRESPONDING TO FIGURE 3.6.**

Case 2: Multiple targets located at random positions;
six harmonics present in output electrical signal;
Sampling parameter S = 2, 4, and 6; 100 iterations; SNR = 0dB

| HARMONIC | LOCATION | | BEARING ANGLE $\psi_o$ ESTIMATION ERROR (DEG) | | |
|---|---|---|---|---|---|
| | $\theta_o$ | $\psi_o$ | | | |
| q | (DEG) | (DEG) | S=2 | S=4 | S=6 |
| 1 | 49 | 38 | -0.261 | +0.236 | +0.001 |
| 2 | 5 | 137 | +0.270 | -0.043 | -1.337 |
| 3 | 77 | 307 | +43.268 | +27.662 | +14.599 |
| 4 | 77 | 307 | +9.620 | +3.789 | +1.100 |
| 5 | 5 | 137 | +0.168 | +1.122 | +0.702 |
| 6 | 49 | 38 | -0.420 | -3.220 | +0.907 |

**TABLE A.5. NUMERICAL DATA CORRESPONDING TO FIGURE 3.7.**

Case 2: Multiple targets located at random positions;
six harmonics present in output electrical signal;
Sampling parameter S = 2, 4, and 6; 100 iterations; SNR = 9dB

| HARMONIC | LOCATION | | DEPRESSION ANGLE $\theta_o$ ESTIMATION ERROR (DEG) | | |
|---|---|---|---|---|---|
| | $\theta_o$ | $\psi_o$ | | | |
| q | (DEG) | (DEG) | S=2 | S=4 | S=6 |
| 1 | 49 | 38 | -0.338 | -0.113 | -0.080 |
| 2 | 5 | 137 | -0.053 | -0.073 | -0.050 |
| 3 | 77 | 307 | -0.425 | +0.280 | -0.192 |
| 4 | 77 | 307 | +1.383 | +0.372 | +1.350 |
| 5 | 5 | 137 | +0.017 | -0.013 | -0.003 |
| 6 | 49 | 38 | -0.447 | +0.059 | +0.022 |

**TABLE A.6. NUMERICAL DATA CORRESPONDING TO FIGURE 3.8.**

Case 2: Multiple targets located at random positions;
six harmonics present in output electrical signal;
Sampling parameter S = 2, 4, and 6; 100 iterations; SNR = 9dB

| HARMONIC | LOCATION | | BEARING ANGLE $\psi_o$ ESTIMATION ERROR (DEG) | | |
|---|---|---|---|---|---|
| | $\theta_o$ | $\psi_o$ | | | |
| q | (DEG) | (DEG) | S=2 | S=4 | S=6 |
| 1 | 49 | 38 | +0.235 | +0.048 | -0.145 |
| 2 | 5 | 137 | +1.288 | +0.263 | +0.725 |
| 3 | 77 | 307 | -0.346 | +0.037 | -0.036 |
| 4 | 77 | 307 | -1.221 | -0.676 | -1.298 |
| 5 | 5 | 137 | +0.648 | -0.148 | -0.538 |
| 6 | 49 | 38 | +0.058 | +0.112 | +0.105 |

**TABLE A.7. NUMERICAL DATA CORRESPONDING TO FIGURE 3.9.**

Case 3: One target located at endfire relative to planar array;
five harmonics present in output electrical signal;
Sampling parameter S = 2, 4, and 6; 100 iterations; SNR = 0dB

| HARMONIC | LOCATION | | DEPRESSION ANGLE $\theta_o$ ESTIMATION ERROR (DEG) | | |
|---|---|---|---|---|---|
| | $\theta_o$ | $\psi_o$ | | | |
| q | (DEG) | (DEG) | S=2 | S=4 | S=6 |
| 1 | 90 | 90 | +7.308 | +7.511 | +7.359 |
| 2 | 90 | 90 | +16.978 | +15.058 | +8.046 |
| 3 | 90 | 90 | +7.594 | +6.119 | +4.723 |
| 4 | 90 | 90 | +13.749 | +7.554 | +2.926 |
| 5 | 90 | 90 | +72.572 | +68.769 | +70.851 |

**TABLE A.8. NUMERICAL DATA CORRESPONDING TO FIGURE 3.10.**

Case 3: One target located at endfire relative to planar array; five harmonics present in output electrical signal; Sampling parameter S = 2, 4, and 6; 100 iterations; SNR = 0dB

| HARMONIC | LOCATION | | BEARING ANGLE $\psi_o$ ESTIMATION ERROR (DEG) | | |
|---|---|---|---|---|---|
| | $\theta_o$ | $\psi_o$ | | | |
| q | (DEG) | (DEG) | S=2 | S=4 | S=6 |
| 1 | 90 | 90 | -0.547 | -0.373 | +0.213 |
| 2 | 90 | 90 | -19.202 | -18.163 | -7.252 |
| 3 | 90 | 90 | +0.168 | -0.038 | -0.094 |
| 4 | 90 | 90 | -3.171 | -0.715 | -0.041 |
| 5 | 90 | 90 | -69.481 | -89.808 | -88.562 |

**TABLE A.9. NUMERICAL DATA CORRESPONDING TO FIGURE 3.11**

Case 3: One target located at endfire relative to planar array; five harmonics present in output electrical signal; Sampling parameter S = 2, 4, and 6; 100 iterations; SNR = 9dB

| HARMONIC | LOCATION | | DEPRESSION ANGLE $\theta_o$ ESTIMATION ERROR (DEG) | | |
|---|---|---|---|---|---|
| | $\theta_o$ | $\psi_o$ | | | |
| q | (DEG) | (DEG) | S=2 | S=4 | S=6 |
| 1 | 90 | 90 | +5.301 | +4.994 | +4.677 |
| 2 | 90 | 90 | +3.523 | +3.175 | +2.932 |
| 3 | 90 | 90 | +3.744 | +2.827 | +2.701 |
| 4 | 90 | 90 | +2.483 | +2.592 | +2.265 |
| 5 | 90 | 90 | +68.938 | +66.092 | +70.858 |

**TABLE A.10. NUMERICAL DATA CORRESPONDING TO FIGURE 3.12.**

Case 3: One target located at endfire relative to planar array; five harmonics present in output electrical signal; Sampling parameter S = 2, 4, and 6; 100 iterations; SNR = 9dB

| HARMONIC | LOCATION | | BEARING ANGLE $\psi_o$ ESTIMATION ERROR (DEG) | | |
|---|---|---|---|---|---|
| | $\theta_o$ | $\psi_o$ | | | |
| q | (DEG) | (DEG) | S=2 | S=4 | S=6 |
| 1 | 90 | 90 | +0.333 | +0.097 | -0.105 |
| 2 | 90 | 90 | -0.030 | -0.123 | +0.088 |
| 3 | 90 | 90 | -0.090 | -0.045 | +0.019 |
| 4 | 90 | 90 | +0.039 | +0.009 | -0.021 |
| 5 | 90 | 90 | -108.012 | -90.250 | -93.038 |

**TABLE A.11. NUMERICAL DATA FOR DEPRESSION ANGLE ESTIMATION ERRORS FOR CASE 4.**

Case 4: Multiple targets; targets one and two share a common spectral line; five harmonics present in output electrical signal; Sampling parameter S = 2, 4, and 6; 100 iterations; no noise

| HARMONIC | LOCATION | | DEPRESSION ANGLE $\theta_o$ ESTIMATION ERROR (DEG) | | |
|---|---|---|---|---|---|
| | $\theta_o$ | $\psi_o$ | | | |
| q | (DEG) | (DEG) | S=2 | S=4 | S=6 |
| 1 | 45 | 0 | +19.683 | +19.683 | +19.683 |
| 2 | 45 | 0 | 0.0 | 0.0 | 0.0 |
| 1 | 45 | 180 | +19.683 | +19.683 | +19.683 |
| 5 | 45 | 180 | 0.0 | 0.0 | 0.0 |
| 3 | 33 | 47 | 0.0 | 0.0 | 0.0 |
| 4 | 33 | 47 | 0.0 | 0.0 | 0.0 |

## TABLE A.12. NUMERICAL DATA FOR BEARING ANGLE ESTIMATION ERRORS FOR CASE 4.

Case 4: Multiple targets; targets one and two share a common spectral line; five harmonics present in output electrical signal; Sampling parameter S = 2, 4, and 6; 100 iterations; no noise

| HARMONIC | LOCATION | | BEARING ANGLE $\psi_o$ ESTIMATION ERROR (DEG) | | |
|---|---|---|---|---|---|
| | $\theta_o$ | $\psi_o$ | | | |
| q | (DEG) | (DEG) | S=2 | S=4 | S=6 |
| 1 | 45 | 0 | -180.00 | -180.00 | -180.00 |
| 2 | 45 | 0 | 0.0 | 0.0 | 0.0 |
| 1 | 45 | 180 | 0.0 | 0.0 | 0.0 |
| 5 | 45 | 180 | 0.0 | 0.0 | 0.0 |
| 3 | 33 | 47 | 0.0 | 0.0 | 0.0 |
| 4 | 33 | 47 | 0.0 | 0.0 | 0.0 |

## LIST OF REFERENCES


1. Reed, F. A., Feintuch, P. L., and Bershad, N. J., "Time Delay Estimation using the LMS Adaptive Filter-Static Behavior," *IEEE Trans. Acoust., Speech, Signal Processing*, vol. ASSP-29, pp. 561–570, June 1981.

2. Reed, F. A., Feintuch, P. L., and Bershad, N. J., "Time Delay Estimation using the LMS Adaptive Filter-Dynamic Behavior," *IEEE Trans. Acoust., Speech, Signal Processing*, vol. ASSP-29, pp. 571–576, June 1981.

3. Reed, F. A., Feintuch, P. L., and Bershad, N. J., "The Application of the Frequency Domain LMS Adaptive Filter to Split Array Bearing Estimation with a Sinusoidal Signal," *IEEE Trans. Acoust., Speech, Signal Processing*, vol. ASSP-33, pp. 61–69, February 1985.

4. Widrow, B., McCool, J., Ball, M., "The Complex LMS Algorithm," *Proc. IEEE*, vol. 63, pp. 719–720, April 1975.

5. Ziomek, L. J. and Chan, F., "Frequency Domain Adaptive Beamforming for Planar Arrays," *Conference Record Twentieth Asilomar Conference on Signals, Systems, and Computers*, pp. 120–124, Pacific Grove, California, 10-12 November 1986.

6. Chan, F., *Two-dimensional Beamforming Using a Frequency Domain Complex Least Mean-Squares (LMS) Adaptive Filter*, Master's and Electrical Engineer Thesis, Naval Postgraduate School, Monterey, California, June 1986.

7. Ziomek, L. J. and Behrle, C. D., *Localization of Multiple Broadband Targets Via Frequency Domain Adaptive Beamforming for Planar Arrays*, paper presented at the Twenty-First Annual Asilomar Conference on Signals, Systems, and Computers, Pacific Grove, California, 2-4 November 1987, in print.

8. Ziomek, L. J., *Underwater Acoustics - A Linear Systems Theory Approach*, Academic Press, Inc., 1985.

No. Copies

## INITIAL DISTRIBUTION LIST

1. Defense Technical Information Center — 2
   Cameron Station
   Alexandria, VA 22304-6145

2. Library, Code 0142 — 2
   Naval Postgraduate School
   Monterey, CA 93943-5002

3. Professor J. P. Powers, Code 62Po — 1
   Department of Electrical & Computer Engineering
   Naval Postgraduate School
   Monterey, CA 93943-5000

4. Professor L. J. Ziomek, Code 62Zm — 3
   Department of Electrical & Computer Engineering
   Naval Postgraduate School
   Monterey, CA 93943-5000

5. Professor M. Tummala, Code 62Tm — 1
   Department of Electrical & Computer Engineering
   Naval Postgraduate School
   Monterey, CA 93943-5000

6. LT C. D. Behrle, USN — 2
   Supervisor of Shipbuilding
   Conversion and Repair, USN
   495 Summer Street
   Boston, MA 02210-2181

7. Chief of Naval Operations — 1
   Code OP-02 Navy Department
   Washington, D.C. 20350

8. Dr. Duncan Sheldon (Surface Sonar) 1
NUSC
Code 3314
New London, CT 06320

END

DATE

FILMED

8-88

DTIC